STING recruits NLRP3 to the ER and deubiquitinates NLRP3 to activate the inflammasome

Wenbiao Wang[1], Dingwen Hu[2], Yuqian Feng[1], Caifeng Wu[1], Aixin Li[2], Yingchong Wang[2], Keli Cheng[2], Mingfu Tian[2], Feng Xiao[2], Qi Zhang[2], Muhammad Adnan Shereen[2], Weijie Chen[1], Pan Pan[1], Pin Wan[1], Weiyong Liu[2], Fang Liu[2], Kailang Wu[2], Geng Li[1], Yingle Liu[1,2], and Jianguo Wu[1,2]*

[1]Guangzhou Key Laboratory of Virology, Institute of Medical Microbiology, Jinan University, Guangzhou 510632, China. [2]State Key Laboratory of Virology, College of Life Sciences, Wuhan University, Wuhan 430072, China.

***Correspondence:** Jianguo Wu, State Key Laboratory of Virology and College of Life Sciences, Wuhan University, Wuhan 430072, P.R. China, Tel.: +86-27-68754979, Fax: +86-27-68754592, Email: jwu@whu.edu.cn

Running title: STING activates the NLRP3 inflammasome

Abstract

One of the fundamental reactions of the innate immune responses to pathogen infection is the release of pro-inflammatory cytokines, including IL-1β, processed by the NLRP3 inflammasome. STING is essential for innate immune responses and inflammasome activation. Here we reveal a distinct mechanism by which STING regulates the NLRP3 inflammasome activation, IL-1β secretion, and inflammatory responses in human cell lines, mice primary cells, and mice. Interestingly, upon HSV-1 infection and cytosolic DNA stimulation, STING binds to NLRP3 and promotes the inflammasome activation through two approaches. First, STING recruits NLRP3 and promotes NLRP3 translocation to the endoplasmic reticulum, thereby facilitating the inflammasome formation. Second, STING interacts with NLRP3 and removes K48- and K63-linked polyubiquitination of NLRP3, thereby promoting the inflammasome activation. Collectively, we demonstrate that the cGAS-STING-NLRP3 signaling is essential for host defense against DNA virus infection.

Keywords: Cyclic GMP-AMP synthase (cGAS)/Herpes simplex virus type 1 (HSV-1)/Interleukine-1β (IL-1β)/Polyubiquitination and deubiquitination/The cGAS-STING pathway

Introduction

The innate immune system detecting pathogens through recognition of molecular patterns is a primary host defense strategy to suppress the infections (Akira et al, 2006). Recognition of pathogens stimuli, known as pathogen-associate molecular patterns (PAMPS), is relied on pattern recognition receptors (PRRs). Several families of PRRs have been described, including the Toll-like receptor (TLR) (Takeuchi & Akira, 2010), RIG-I-like receptor (RLR) (Yoneyama et al., 2004), NOD-like receptor (NLR) (Ting et al, 2008), and C-type lectin receptor (CLR) (Hardison & Brown, 2012). The NLRs involved in the assembly of large protein complexes referred to as inflammasomes are emerging as a major route by which the innate immune system responds to pathogen infections (Schroder & Tschopp, 2010). One of the fundamental reactions of the innate immunity is the procession and release of pro-inflammatory cytokines, including interleukine-1β (IL-1β), a pleiotropic cytokine playing crucial roles in inflammatory responses in addition to instructing immune responses (Dinarello, 2009). The best-characterized inflammasomes is the NLRP3 inflammasome, which consists of three major components: a cytoplasmic sensor NLRP3 (NACHT, LRR and PYD domains-containing protein 3), an adaptor ASC (apoptosis-associated speck-like protein with CARD domain), and an interleukin-1β-converting enzyme pro-Caspase-1 (cysteinyl aspartate-specific proteinase-1) (Schroder & Tschopp, 2010). NLRP3 and ASC together promote the cleavage of pro-Casp-1 to generate active subunits p20 and p10, which regulate IL-1β maturation (Martinon et al, 2004).

The stimulator of interferon genes (STING) has the essential roles in innate immune response against pathogen infections (Ishikawa et al, 2009). Upon binding of cytoplasmic DNA, cyclic

GMP-AMP synthase (cGAS) catalyzes the formation of cyclic guanosine monophosphate-adenosine monophosphate (cGAMP) by binding to STING. STING subsequently co-localizes with TBK1 and IRF3, leading to induction of type I IFNs, and recruits TRAF6 and TBK1 or TRAF3 and IKKα to activate the NF-κB pathway (Abe & Barber, 2014; Wu et al., 2013). In human myeloid cells, STING is involved in cytosolic DNA induced-NLRP3 inflammasome activation (Gaidt et al, 2017), and in mice BMDMs, STING is required for pathogen-induced inflammasome activation and IL-1β secretion (Webster et al., 2017; Swanson et al., 2017).

We explored how STING regulates the NLRP3 inflammasome and reveal a distinct mechanism underlying such regulation upon herpes simplex virus type 1 (HSV-1) infection and cytosolic DNA stimulation. HSV-1 causes various mild clinical symptoms, while in immunocompromized and neonates individuals, it can cause herpes simplex encephalitis, which may lead to death or result in some neurological problems (Roizman, 2013). But the detailed mechanisms by which HSV-1 regulates the NLRP3 inflammasome are largely unknown. We demonstrate that HSV-1-induced NLRP3 inflammasome activation is dependent on the cGAS-cGAMP-STING pathway. STING recruits and promotes NLRP3 translocation to the endoplasmic reticulum, and binds and removes NLRP3 polyubiquitination, thereby promoting the inflammasome activation. We propose that the cGAS-cGAMP-STING-NLRP3 axis is essential for host defense against DNA virus infection.

Results

STING interacts with NLRP3 to facilitate the inflammasome activation.

We initially determined the correlation between STING and NLRP3, and showed that STING and NLRP3 interacted with each other in human embryonic kidney (HEK293T) cells (Fig 1A, B). The NLRP3 inflammasome consists of three major components, NLRP3, ASC, and pro-Casp-1 (Schroder & Tschopp, 2010). We explored whether STING interacts with ASC and/or pro-Casp-1, and clearly revealed that STING interacted with NLRP3, but not with ASC or pro-Casp-1 (Fig 1C). NLRP3 protein harbors several prototypic domains, including PYRIN domain (PYD), NACHT-associated domain (NAD), and Leucine rich repeats (LRR) (Ye & Ting, 2008). Next, the domain of NLRP3 involved in the interaction with STING was determined by evaluating the plasmids encoding NLRP3, PYRIN, NACHT, or LRR (Figure 1D) as described previously (Wang et al, 2018). Like NLRP3, NACHT and LRR interacted with STING, but PYRIN failed to interact with STING (Figure 1E), and consistently, STING interacted with NLRP3, NACHT, and LRR (Fig 1F, lanes 2, 6 and 8), but not with PYRIN (Fig 1F, lane 4). In another hand, STING comprises five putative transmembrane (TM) regions (Ishikawa & Barber, 2008). The domain of STING required for the interaction with NLRP3 was assessed by analyzing plasmids encoding wild-type (WT) STING and seven truncated proteins (Fig 1G). Like WT STING(1–379aa) (Fig 1H, lane 9), the truncated proteins STING(1–160aa), STING(1–240aa), STING(41–379aa), STING(81–379aa), and STING(111–379aa) interacted strongly with NLRP3 (Fig 1H, lane 2–6), STING(151–379aa) associated weakly with NLRP3 (Fig 1H, lane 7), but STING(211–379aa) failed to interact with NLRP3 (Fig 1H, lane 8), indicating that TM5 (151–160aa) of STING is involved in the interaction

with NLRP3.

The role of STING in the regulation of the NLRP3 inflammasome was explored by using a pro-Casp-1 activation and pro-IL-1β cleavage cell system as established previously (Wang et al., 2017). In this system (NACI), HEK293T cells were co-transfected with plasmids encoding NLRP3, ASC, pro-Casp1, and pro-IL-1β. In the NACI cells, IL-1β secretion was stimulated by STING(1–160aa), STING(1–240aa), STING(41–379aa), or STING (Fig 1I, lane 2–4 and 9), but not by STING(81–379aa), STING(111–379aa), STING(151–379aa) or STING(211–379aa) (Fig 1I, lane 5–8), suggesting that TM2 (41–81aa) of STING is required for the induction of IL-1β secretion. Notably, STING promoted the NLRP3-ASC interaction (Fig 1J), an indicator of the inflammasome assembly (Compan et al., 2012) and enhanced NLRP3-mediated ASC oligomerization (Fig 1K), which is critical for inflammasome activation (Shenoy et al., 2012). Moreover, in HEK293T cells (Fig 1L) and HeLa cells (Fig 1M), NLRP3 and STING co-localized and formed large spots in the cytosol (Fig 1L and M), an indication of the NLRP3 inflammasome formation ((Martinon et al., 2009). Taken together, STING interacts with NLRP3 through TM5 domain and promotes the assembly and activation of the NLRP3 inflammasome through TM2 domain.

HSV-1 infection promotes the STING-NLRP3 interaction.

STING plays a key role in host innate immune response in response to pathogen infections and cytosolic DNA simulation (Ishikawa & Barber, 2008). We evaluated the effects of HSV-1 infection and HSV120 transfection, a biotinylated dsDNA representing the genomes of HSV-1 that efficiently induces STING-dependent type I IFN production as reported previously (Abe et al., 2013) on the STING-NLRP3 interaction. In TPA-differentiated human leukemic monocyte (THP-1) macrophages,

HSV-1 infection facilitated endogenous NLRP3-STING interaction and promoted endogenous STING-NLRP3 interaction (Fig 2A, B). In HEK293T cells and HeLa cells (Fig 2D), the STING-NLRP3 interaction was enhanced upon HSV-1 infection (Fig 2C, D). Similarly, in TPA-differentiated THP-1 macrophages, HEK293T cells, and HeLa cells, the NLRP3-STING interaction was promoted by HSV120 transfection (Fig 2E−G). Moreover, in primary mouse embryo fibroblasts (MEFs), HSV-1 infection and HSV120 transfection facilitated endogenous STING-NLRP3 interaction (Fig 2H). Collectively, HSV-1 infection and HSV120 transfection facilitate the interaction of STING with NLRP3.

HSV-1 infection induces IL-1β expression and secretion.

Next, we explored whether HSV-1 infection and HSV120 transfection regulate the NLRP3 inflammasome activation. In TPA-differentiated THP-1 macrophages, endogenous IL-1β secretion was induced by Nigericin (a positive control for the inflammasome activation) and HSV-1 (Fig 3A, B). Consistently, IL-1β maturation and Casp-1 cleavage, as well as pro-IL-1β production were activated upon HSV-1 infection (Fig 3C, D). Notably, IL-1β mRNA was not induced by Nigericin but induced upon HSV-1 infection (Fig 3E, F) and HSV-1 ICP27 mRNA was expressed in the infected cells (Fig 3G, H). Similarly, in TPA-differentiated THP-1 macrophages, IL-1β secretion was induced by Nigericin and facilitated by HSV120 (Fig 3I). IL-1β maturation and Casp-1 cleavage and pro-IL-1β production were stimulated by Nigericin and promoted by HSV120 (Fig 3J). IFN-β mRNA expression was not induced by Nigericin but activated by HSV120 (Fig 3K), demonstrating that HSV120 is effective in the cells. Moreover, in mice primary MEFs, endogenous IL-1β secretion was induced by ATP (a positive control), promoted upon HSV-1 infection, and

enhanced by HSV120 stimulation (Fig 3L, M). HSV-1 ICP27 mRNA was detected in the cells (Fig 3N), suggesting that HSV-1 is replicated. IFN-β mRNA was not induced by ATP but activated by HSV120 in the cells (Fig 3O), demonstrating that HSV120 is effective. Therefore, IL-1β expression and secretion are induced upon DNA virus infection and cytosolic DNA stimulation.

The NLRP3 inflammasome is required for HSV-1-induced IL-1β activation.

Accordingly, we determined whether the NLRP3 inflammasome is required for HSV-1 in the induction of IL-1β activation. Initially, the effects of glybenclamide (NLRP3 inhibitor) and Ac-YVAD-cmk (Casp-1 inhibitor) (Wang et al., 2015) on HSV-1-mediated IL-1β activation were evaluated. In TPA-differentiated THP-1 macrophages, IL-1β secretion (Fig 4A, C) as well as IL-1β (p17) cleavage and Casp-1(p20 and p22) maturation (Fig 4B, D) activated by Nigericin and HSV-1 were significantly attenuated by glybenclamide (Fig 4A, B) or Ac-YVAD-cmk (Fig 4C, D). HSV-1 ICP27 mRNA was expressed in infected cells (Fig 4E, F), indicating that HSV-1 is replicated.

In addition, the role of endogenous NLRP3 inflammasome in HSV-1-induced IL-1β activation was assessed in THP-1 cell lines stably expressing negative control shRNA (sh-NC) and shRNAs (sh-NLRP3, sh-ASC and sh-Casp-1) targeting the NLRP3 inflammasome components. Notably, IL-1β secretion (Fig 4G, I) as well as IL-1β (p17) cleavage and Casp-1 (p20 and p22) maturation (Fig 4H, J, top) induced by Nigericin (Fig 4G, H) or HSV-1 (Fig 4I, J) were attenuated by sh-NLRP3, sh-ASC, and sh-Casp-1. The NLRP3, ASC, and pro-Casp-1 proteins were own-regulated by sh-NLRP3, sh-ASC, and sh-Casp-1 stable cells, respectively (Fig 4H, J, bottom), indicating that shRNAs are effective in the cells. HSV-1 ICP27 mRNA was expressed in infected cells (Fig 4K), confirming that HSV-1 is replicated in the cells.

Moreover, the direct role of NLRP3 in the regulation of HSV-1-induced IL-1β secretion was determined in primary MEFs of C57BL/6 WT pregnant mice and NLRP3$^{-/-}$ pregnant mice. NLRP3 protein was detected in WT mice primary MEFs, but not in NLRP3$^{-/-}$ mice primary MEFs (Fig 4L), indicating that NLRP3 is knocked out in the null mice. IL-1β secretion was induced by ATP and HSV-1 in WT mice primary MEFs but not in NLRP3$^{-/-}$ mice primary MEFs (Fig 4M). HSV-1 ICP27 mRNA was expressed in infected cells, indicating that HSV-1 is replicated in the cells (Fig 4N). Collectively, inhibition, knock-down, and knock-out of the NLRP3 inflammasome components lead to the repression of IL-1β secretion and Casp-1 maturation, therefore the NLRP3 inflammasome is required for HSV-1-induced activation of IL-1β.

STING recruits NLRP3 to the ER to promote the inflammasome formation.

STING predominantly resides in the endoplasmic reticulum (ER) to regulate innate immune signaling processes (Ishikawa & Barber, 2008). Here we evaluated whether STING recruits NLRP3 to ER and activates the inflammasome. In HeLa cells, NLRP3 alone diffusely distributed in the cytoplasm and STING alone located in the ER (as indicated by the ER marker, ER blue), while NLRP3 and STING together co-localized and distributed in the ER to form specks (Fig 5A), which is an indication of the NLRP3 inflammasome complex formation (Martinon et al., 2009), suggesting that STING recruits NLRP3 to the ER and promotes the inflammasome formation. In addition, NLRP3 diffusely distributed in the cytosol of untreated cells, but formed distinct specks upon HSV-1 infection or HSV120 transfection (Fig 5B). Moreover, NLRP3 diffusely distributed in the cytosol of untreated cells, while upon HSV-1 infection or HSV120 transfection, NLRP3 forms distinct specks in the ER as indicated by Calnexin (ER protein) (Fig 5C) and ER blue (ER marker)

(Fig 5D). Notably, in transfected HeLa cells, NLRP3, STING, and Calnexin were detected in whole cell lysate (WCL) and purified ER fraction, and interestingly, NLRP3 abundance was enhanced by STING in purified ER fraction (Fig 5E). Similarly, in mock-infected THP-1 macrophages and mice primary MEFs, NLRP3, STING, and Calnexin were detected in WCL and purified ER, and NLRP3 abundance was increased in the ER upon HSV-1 infection (Fig 5F, G). Therefore, STING, HSV-1, and HSV120 facilitate the NLRP3 inflammasome formation in the ER.

Moreover, the effect of endogenous STING on NLRP3 translocation to the ER was further determined by using shRNA targeting STING (sh-STING). Hela cells stably expressing sh-NC or sh-STING were generated, and then transfected with Flag-NLRP3 and infected with HSV-1 or transfected with HSV120. In the absence of sh-STING, NLRP3 diffusely distributed in the cytosol of untreated cells and formed distinct specks in the ER, as indicated by Calnexin and ER Blue (Fig 5H, I, top), upon HSV-1 infection or HSV120-transfection, however, in the presence of sh-STING, NLRP3 failed to form specks upon HSV-1 infection or HSV120 transfection (Fig 5H, I, bottom), indicating that STING knock-down leads to the repression of HSV-1-induced formation of the NLRP3 inflammasome. In addition, NLRP3, Calnexin, and STING were detected in WCL and purified ER fraction of Hela cells (Fig 5J), THP-1 cells (Fig 5K) and mice primary MEFs (Fig 5L), and notably, NLRP3 level was higher in purified ER fraction upon HSV-1 infection in sh-NC stable cells (Fig 5J–L, lane 6 vs. 5) as compared with sh-STING stable cells (Fig 5J–L, lane 8 vs. 7), suggesting that STING knock-down results in the attenuation of NLRP3 translocation to the ER upon HSV-1 infection. We also confirmed that STING abundance was down-regulated by sh-STING (Fig 5J–L). Collectively, STING recruits NLRP3 to the ER and promotes the NLRP3 inflammasome formation upon HSV-1 infection and cytosolic DNA stimulation.

STING deubiquitinates NLRP3 to activate the NLRP3 inflammasome.

The deubiquitination of NLRP3 is required for the NLRP3 inflammasome activation (Juliana et al., 2012). We next investigated whether STING plays a role in the deubiquitination of NLRP3, thereby facilitating the inflammasome activation. Interestingly, NLRP3 polyubiquitination catalyzed by HA-UB, HA-UB(K48R), or HA-Ub(K63R) was repressed by STING (Fig 6A, B). We also revealed that NLRP3 polyubiquitination catalyzed by HA-UB, HA-UB(K48O) (ubiquitin mutant that only retains a single lysine residue), or HA-UB(K63O) (ubiquitin mutant that only retains a single lysine residue) was suppressed by STING (Fig 6C). These results reveal that STING removes K48- and K63-linked polyubiquitination of NLRP3.

In addition, we examined whether HSV-1 infection and HSV120 transfection regulate the deubiquitination of NLRP3. Notably, NLRP3 polyubiquitination catalyzed by HA-UB was attenuated upon HSV-1 infection (Fig 6D) or by HSV120 transfection (Fig 6E). In THP-1 differentiated macrophages, UB-catalyzed (Fig 6F, top), K48-linked (Fig 6F, middle), and K63-linked (Fig 6F, bottom) polyubiquitination of endogenous NLRP3 was repressed upon HSV-1 infection; and UB-catalyzed polyubiquitinion of endogenous NLRP3 was repressed by HSV120 (Fig 6G). Moreover, in mice primary MEFs, UB-catalyzed ployubiquitination of endogenous NLRP3 was attenuated upon HSV-1 infection (Fig 6H). Therefore, HSV-1 infection and HSV120 stimulation promote the deubiquitination of endogenous NLRP3. Moreover, upon HSV-1 infection, the ployubiquitination of endogenous NLRP3 was attenuated in the presence of sh-NC but relatively unaffected in the presence of sh-STING (Fig 6I), indicating that STING knock-down leads to repression of NLRP3 deubiquitination. Taken together, STING removes K48- and K63-linked

polyubiquitination of NLRP3 to promote the inflammasome activation upon HSV-1 infection and cytosolic DNA stimulation.

STING is required for the NLRP3 inflammasome activation upon DNA virus infection.

Since STING recruits NLRP3 to the ER and removes NLRP3 deubiquitination upon HSV-1 infection, we speculated that STING may play a role in HSV-1-induced NLRP3 inflammasome activation. The effect of STING knock-down on HSV-1-induced NLRP3 inflammasome activation was initially examined in THP-1 cells stably expressing sh-STING. Endogenous IL-1β secretion as well as IL-1β (p17) cleavage and Casp-1 (p20 and p22) maturation induced by HSV-1 were significantly attenuated by sh-STING (Fig 7A, B). HSV-1 ICP27 mRNA was detected in HSV-1 infection cells (Fig 7C), indicating that HSV-1 is replicated. Additionally, endogenous IL-1β secretion, IL-1β (p17) maturation, and Casp-1 (p20 and p22) cleavage induced by DNA90, HSV120, or HSV-1 were suppressed by sh-STING (Fig 7D, E). Thus, STING knock-down leads to the suppression of IL-1β secretion and Casp-1 maturation upon DNA virus infection and cytosolic DNA stimulation.

Accordingly, we determine whether STING plays a specific role in the NLRP3 inflammasome activation mediated by DNA virus. THP-1 cells stably expressing sh-STING were differentiated to macrophages, and then treated with Nigericin or infected with HSV-1. Notably, sh-STING significantly attenuated endogenous IL-1β secretion as well as L-1β (p17) maturation and Casp-1 (p20 and p22) cleavage induced upon HSV-1 infection, but had no effect on IL-1β secretion or IL-1β (p17) maturation and Casp-1 (p20 and p22) cleavage induced by Nigericin stimulation (Fig 7F, G). HSV-1 ICP27 mRNA was detected in HSV-1 infection cells (Fig 7H), indicating that HSV-1 is

255 replicated in the cells. Moreover, we explored whether STING plays roles in the NLRP3
256 inflammasome activation induced by RNA viruses. THP-1 differentiated macrophages stably
257 expressing sh-STING were infected with RNA viruses, Sendai virus (SeV) and Zika virus (ZIKV),
258 or with HSV-1. Interestingly, endogenous IL-1β secretion as well as IL-1β (p17) maturation and
259 Casp-1 (p20 and p22) cleavage were induced upon the infections of the three viruses, however,
260 HSV-1-mediated induction was attenuated by sh-STING, but SeV- or ZIKV-mediated inductions
261 were not affected by sh-STING (Fig 7I, J). SeV P mRNA, ZIKV mRNA, and HSV-1 ICP27 mRNA
262 were detected in infected cells, respectively (Fig 7K–M). Taken together, STING plays specific
263 roles in the NLRP3 inflammasome activation upon DNA virus infection or cytosolic DNA
264 stimulation, but has no effect on the inflammasome activation induced by RNA virus infection or
265 Nigericin stimulation.
266
267 **NLRP3 is critical for host defense against HSV-1 infection in mice.**
268 To gain insights into the biological function of NLRP3 *in vivo*, we analyzed C57BL/6 NLRP3$^{+/+}$
269 WT mice and C57BL/6 NLRP3$^{-/-}$ deficiency mice. Notably, HSV-1-infected NLRP3$^{-/-}$ mice began to
270 die at 5 days post-infection and all infected mice died at 7 days post-infection, while infected WT
271 mice began to die at 7 days post-infection and 30% WT mice was survival after 11 days
272 post-infection (Fig 8A). The body weights of infected NLRP3$^{-/-}$ mice decreased continuously until
273 died, while the body weights of infected WT mice gradually decreased until 7 days post-infection
274 and then gradually increased (Fig 8B). Thus, NLRP3 deficiency mice are more susceptibility to
275 HSV-1 infection and exhibit early onset of death upon the infection.
276 Notably, in the mice blood, IL-1β secretion was induced upon HSV-1 infection in WT mice,

277 whereas it was not induced in NLRP3$^{-/-}$ mice (Fig 8C), IL-1β mRNA level was higher in WT mice
278 as compared with NLRP3$^{-/-}$ mice (Fig 8D), IL-6 mRNA and TNF-α mRNA were no significant
279 difference between WT and NLRP3$^{-/-}$ mice (Fig 8E, F), and HSV-1 UL30 mRNA was expressed in
280 infected WT and NLRP3$^{-/-}$ mice (Fig 8G). These results indicate that NLRP3 deficiency leads to the
281 repression of IL-1β expression and secretion in mice. Interestingly, in HSV-1 infected mice lung and
282 brain, IL-1β mRNA and IL-6 mRNA were significantly higher in WT mice as compared with
283 NLRP3$^{-/-}$ mice (Fig 8H, I, K and L), however, the viral titers were much lower in WT mice as
284 compared with NLRP3$^{-/-}$ mice (Fig 8J, M), suggesting that NLRP3 deficiency results in the
285 attenuation of IL-1β expression and the promotion of HSV-1 replication in mice lung and brain.
286 Moreover, Hematoxylin and Eosin (H&E) staining showed that more infiltrated neutrophils and
287 mononuclear cells were detected in the lung and brain of infected WT mice as compared with
288 NLRP3$^{-/-}$ mice (Fig 8N), and immunohistochemistry (IHC) analysis revealed that IL-1β protein
289 level was higher in the lung and brain of infected WT mice as compared with NLRP3$^{-/-}$ mice (Fig
290 8O), revealing that NLRP3 deficiency mice are more susceptibility to HSV-1 infection and elicit
291 weak inflammatory responses. Collectively, we propose that NLRP3 is essential for host defense
292 against HSV-1 infection by facilitating IL-1β activation (Fig 9).
293

Discussion

This study reveals a distinct mechanism by which the cGAS-STING-NLRP3 pathway promotes the NLRP3 inflammasome activation and IL-1β secretion upon DNA virus infection and cytosolic DNA stimulation. The cGAS-STING pathway mediates immune defense against infection of DNA-containing pathogens and detects tumor-derived DNA and generates intrinsic antitumor immunity (Chen et al., 2016; Wu et al., 2013). More recent studies reported that in human monocytes, the cGAS-STING pathway is essential for cytosolic DNA induced-NLRP3 inflammasome (Gaidt et al., 2017) and in mice BMDMs, the cGAS-STING pathway is required for Chlamydia trachomatis-induced inflammasome activation and IL-1β secretion (Webster et al., 2017; Swanson et al., 2017). Our results are consistent with the reports and further support that cGAS-STING pathway is essential not only for cytosolic DNA induced- or Chlamydia trachomatis-induced NLRP3 inflammasome activation, but also for DNA virus-induced NLRP3 inflammasome activation. This study also further reveals that the cGAS-STING pathway is required for the NLRP3 inflammasome activation not only in human monocytes and mice BMDMs, but also in human embryonic kidney cells (HEK293T), Hela cells, human leukemic monocytes/macrophages (THP-1), and mice primary mouse embryo fibroblasts (MEFs). More interestingly, our results reveal a distinct mechanism underlying STING-mediated NLRP3 inflammasome activation, and demonstrate for the first time that STING binds to NLRP3 and promotes the inflammasome activation through two approaches. First, STING binds to and recruits NLRP3 to the ER to promote the formation of the NLRP3 inflammasome. Second, STING interacts with NLRP3 and removes K48- and K63-linked polyubiquitination of NLRP3 to induce the activation of the NLRP3

316 inflammasome. Notably, upon HSV-1 infection and HSV120 stimulation, STING binds to NLRP3,
317 promotes the NLRP3-ASC interaction (an indicator of inflammasome complex assembly) (Compan
318 et al., 2012), facilitates NLRP3-mediated ASC oligomerization (a critical step for inflammasome
319 activation) (Shenoy et al., 2012), enhances NLRP3 to form specks (an indicator of inflammasome
320 activation) (Martinon et al, 2009), and enhances IL-1β secretion (a fundamental reaction of the
321 inflammatory responses) (Dinarello, 2009). Collectively, the cGAS-STING-NLRP3 pathway plays
322 key roles in the NLRP3 inflammasome activation and IL-1β secretion upon DNA virus infection
323 and cytosolic DNA stimulation.

324 Notably, STING knock-down attenuates the NLRP3 inflammasome activation mediated upon
325 DNA virus infection or cytosolic DNA stimulation, but has no effect on the NLRP3 inflammasome
326 activation induced by RNA virus infection or Nigericin induction. Many RNA viruses induce the
327 NLRP3 inflammasome activation, including influenza A virus (IAV) (Kanneganti et al., 2006),
328 Vesicular mastitis virus (VSV) and Encephalomyocarditis virus (EMCV) (Rajan et al., 2011),
329 Measles virus (MV) (Komune et al., 2011), West Nile virus (WNV) (Ramos et al., 2012), Rabies
330 virus (RV) (Lawrence et al., 2013), Hepatitis C virus (HCV) (Negash et al., 2013), Dengue virus
331 (DENV) (Hottz et al., 2013), Enterovirus 71 (EV71) (Wang et al., 2017) and Zika virus (ZIKV)
332 (Wang et al., 2018). Some DNA viruses also regulate the NLRP3 inflammasome activation, such as
333 Adenovirus (AdV) (Muruve et al., 2008) and HSV-1 (Johnson et al., 2013). HSV-1 VP22 inhibits
334 AIM2-denpendent inflammasome activation so that HSV-1 infection of macrophages-induced
335 inflammasome activation is AIM2-independent (Maruzuru et al., 2018). Here, we demonstrate that
336 the cGAS-STING-NLRP3 pathway is required for HSV-1-induced NLRP3 inflammasome
337 activation and critical for host defense against DNA virus infection.

The mechanisms of NLRP3 inflammasome activation have been intensely studied. The mitochondria-associated adaptor protein (MAVS) promotes NLRP3 mitochondrial localization and the inflammasome activation (Subramanian et al., 2013). PtdIns4P mediates the NLRP3 inflammasome activation in trans-Golgi network (TGN) (Chen & Chen, 2018). NLRP3 associates with SCAP-SREBP2 to form a ternary complex that translocates to the Golgi apparatus for optimal inflammasome assembly (Guo et al., 2018). Here we find that STING promotes NLRP3 translocation to the ER and facilitates the inflammasome activation. Moreover, post-translational modifications of NLRP3 are critical for its activation, including phosphorylation (Song & Li, 2018), SUMOylation (Barry et al., 2018), and ubiquitination (Py et al., 2013). MARCH7 and TRIM31 facilitate NLRP3 ubiquitination and proteasomal degradation (Song et al., 2016; Yan et al., 2015). Pellino2 promotes K63-linked ubiquitination of NLRP3 as part of the priming phase (Humphries et al., 2018). Interestingly, we demonstrate that STING removes K48- and K63-linked ubiquitination of NLRP3 to promote the inflammasome activation, and reveal that HSV-1 infection induces STING-mediated deubiquitination of NLRP3.

Moreover, NLRP3 is related to many human diseases. Fibrillar amyloid-β peptide, the major component of Alzheimer's disease brain plaques, facilitates the NLRP3 inflammasome activation (Halle et al., 2008). Monosodium urate (MSU) crystals induce the autoinflammatory disease gout and activate the NLRP3 inflammasome (Martinon et al., 2006). NLRP3, IL-1β, reactive oxygen species (ROS), and TXNIP are implicated in the type 2 diabetes mellitus (T2DM) pathogenesis (Schroder et al., 2010). Our study gains insights into the biological function of the cGAS-STING-NLRP3 pathway in host defense against HSV-1 infection in mice. NLRP3 deficiency mice are more susceptibility to HSV-1 infection, exhibit early onset of death upon infection,

360 represses IL-1β secretion, and elicits robust inflammatory responses in the tissues. Collectively,
361 these results demonstrate that NLRP3 is essential for host defense against HSV-1 infection by
362 inducting IL-1β expression and secretion.

363 In conclusion, we reveal a distinct mechanism underlying the regulation of the NLRP3
364 inflammasome activation upon DNA virus infection. In this model, STING (the central molecule of
365 the antiviral and inflammatory immune pathways) interacts with NLRP3 (the key component of the
366 inflammasomes), removes NLRP3 polyubiquitination, recruits NLRP3 to the ER, and facilitates the
367 NLRP3 inflammasome activation, thereby inducing IL-1β secretion upon DNA virus infection and
368 cytosolic DNA stimulation.

369

Materials and Methods

Animal study

C57BL/6 WT mice were purchased from Hubei Research Center of Laboratory Animals (Wuhan, Hubei, China). C57BL/6 NLRP3$^{-/-}$ mice were kindly provided by Dr. Di Wang of Zhejiang University School of Medicine, China.

The primary mouse embryo fibroblasts (MEFs) were prepared from pregnancy mice of C57BL/6 WT mice and C57BL/6 NLRP3$^{-/-}$ mice in E14 and cultured in Dulbecco modified Eagle medium (DMEM) containing 10% heat-inactivated fetal bovine serum (FBS).

Ethics statement.

All animal studies were performed in accordance with the principles described by the Animal Welfare Act and the National Institutes of Health Guidelines for the care and use of laboratory animals in biomedical research. All procedures involving mice and experimental protocols were approved by the Institutional Animal Care and Use Committee (IACUC) of the College of Life Sciences, Wuhan University.

Cell lines and cultures

African green monkey kidney epithelial (Vero) cells, human cervical carcinoma (Hela) cells, and human embryonic kidney 293T (HEK 293T) cells were purchased from American Type Culture Collection (ATCC) (Manassas, VA, USA). Human acute monocytic leukemia (THP-1) cells were gift from Dr. Jun Cui of State Key Laboratory of Biocontrol, School of Life Sciences, Sun Yat-Sen

University, Guangzhou 510275, China. THP-1 cells were cultured in RPMI 1640 medium supplemented with 10% heat-inactivated fetal bovine serum (FBS), 100 U/ml penicillin, and 100 μg/ml streptomycin sulfate. Vero, Hela and HEK293T cells were cultured in Dulbecco modified Eagle medium (DMEM) purchased from Gibco (Grand Island, NY, USA) supplemented with 10% FBS, 100 U/ml penicillin and 100 μg/ml streptomycin sulfate. Vero, Hela, HEK293T and THP-1 cells were maintained in an incubator at 37°C in a humidified atmosphere of 5% CO_2.

Reagents

Lipopolysaccharide (LPS), adenosine triphosphate (ATP), Endoplasmic Reticulum Isolation Kit (ER0100), phorbol-12-myristate-13-acetate (TPA) and dansylsarcosine piperidinium salt (DSS) were purchased from Sigma-Aldrich (St. Louis, MO, USA). RPMI 1640 and Dulbecco modified Eagle medium (DMEM) were obtained from Gibco (Grand Island, NY, USA). Nigericin and Ac-YVAD-cmk were obtained from InvivoGene Biotech Co., Ltd. (San Diego, CA, USA). Antibody against Flag (F3165), HA (H6908) and monoclonal mouse anti-GAPDH (G9295) were purchased from Sigma (St. Louis, MO, USA). Monoclonal rabbit anti-NLRP3 (D2P5E), Ubiquitin mouse mAb (P4D1), monoclonal rabbit anti-K63-linkage Specific Polyubiquitin (D7A11), monoclonal rabbit anti-K48-linkage Specific Polyubiquitin (D9D5), monoclonal rabbit anti-STING(D2P2F), monoclonal rabbit anti-calnexin(C5C9), monoclonal rabbit anti-IL-1β (D3U3E), IL-1β mouse mAb (3A6) and monoclonal rabbit anti-Caspase-1 (catalog no. 2225) were purchased from Cell Signaling Technology (Beverly, MA, USA). Monoclonal mouse anti-ASC (sc-271054) and polyclonal rabbit anti-IL-1β (sc-7884) were purchased from Santa Cruz Biotechnology (Santa Cruz, CA, USA). Monoclonal mouse anti-NLRP3 (AG-20B-0014-C100) was purchased from Adipogen to detection

414 endogenous NLRP3 in THP1 cells and primary MEFs. Lipofectamine 2000, ER-Tracker™
415 Blue-White DPX (E12353), normal rabbit IgG and normal mouse IgG were purchased from
416 Invitrogen Corporation (Carlsbad, CA, USA).
417
418 **Viruses**
419 Herpes simplex virus 1 (HSV-1) strain and Sendai virus (SeV) strain were gifts from Dr. Bo
420 Zhong of Wuhan University. Zika virus (ZIKV) isolate z16006 (GenBank accession number
421 KU955589.1) was used in this study. Vero cells were maintained at 37°C in DMEM (GIBCO)
422 supplemented with 10% heat-inactivated FBS with penicillin/streptomycin (GIBCO) (Grand Island,
423 NY, USA). HSV-1 stocks were propagated in Vero cells for 36 h at 0.03 MOI. The infected cells
424 were harvested and resuspended by PBS. HSV-1 was collected after three times of freezing and
425 thawing in the infected cells and titrated by plaque assay in 12-well plates in Vero cells.
426
427 **Plaque assay**
428 Vero cells were cultured in a 12-well plate at a density of 2×10^5 cells per well, and infected
429 with 100 μl serially diluted HSV-1 supernatant for 2 h. Then, the cells were washed by PBS and
430 then immediately replenished with plaque medium supplemented with 1% carboxylmethylcelluose.
431 The infected Vero cells were incubated for 2–3 days. After the incubation, plaque medium was
432 removed and cells were fixed and stained with 4% formaldehyde and 0.5% crystal violet.
433
434 **THP-1 macrophages stimulation**
435 THP-1 cells were differentiated into macrophages with 100 ng/ml

phorbol-12-myristate-13-acetate (TPA) for 12 h, and cells were cultured for 24 h without TPA. Differentiated cells were then stimulated with HSV-1 infection, HSV120 transfection, DNA90 transfection, Sendai virus (SeV) infection, Zika virus (ZIKV) infection, or Nigericin treatment. Supernatants were collected for measurement of IL-1β by Enzyme-linked immunosorbent assay (ELISA). Cells were harvested for real-time PCR or immunoblot analysis.

Plasmid construction

The cDNAs encoding human STING, NLRP3, ASC, pro-Casp-1, and IL-1β were obtained by reverse transcription of total RNA from TPA-differentiated THP-1 cells, followed by PCR using specific primers. The cDNAs were sub-cloned into pcDNA3.1(+) and pcagg-HA vector. The pcDNA3.1(+)-3×Flag vector was constructed from pcDNA3.1(+) vector through inserting the 3×Flag sequence between the NheI and HindIII site. Following are the primers used in this study. Flag-NLRP3: 5’-CGCGGATCCATGAAGATGGCAAGCACCCGC-3’, 5’-CCGCTCGAGCTACCAAGAAGGCTCAAAGAC-3’; Flag-ASC: 5’-CCGGAATTCATGGGGCGCGCGCGCGACGCCAT-3’, 5’-CCGCTCGAGTCAGCTCCGCTCCAGGTCCTCCA-3’; Flag-Casp-1: 5’-CGCGGATCCATGGCCGACAAGGTCCTGAAG-3’, 5’-CCGCTCGAGTTAATGTCCTGGGAAGAGGTA-3’; Flag-IL-1β: 5’-CCGGAATTCATGGCAGAAGTACCTGAGCTC-3’, 5’-CCGCTCGAGTTAGGAAGACACAAATTGCAT-3’; Flag-STING: 5’-CCGGAATTCTATGCCCCACTCCAGCCTGCA-3’, 5'-CCGCTCGAGTCAAGAGAAATCCGTGCGGAG-3’. HA-NLRP3:

458 5’-TACGAGCTCATGAAGATGGCAAGCACCCGC-3’,

459 5’-CCGCTCGAGCCAAGAAGGCTCAAAGACGAC-3’; HA-ASC:

460 5’-CCGGAATTCATGGGGCGCGCGCGCGACGCC-3’,

461 5’-CCGCTCGAGGCTCCGCTCCAGGTCCTCCAC-3’; HA-Casp-1:

462 5’-CCGGAATTCATGGCCGACAAGGTCCTGAAG-3’,

463 5’-CCGCTCGAGATGTCCTGGGAAGAGGTAGAA-3’.

464 The STING truncates was cloned into pcDNA3.1(+) and the PYRIN, NACHT, and LRR

465 domain of NLRP3 protein was cloned into pcDNA3.1(+) and pcaggs-HA vector using specific

466 primers, which are listed as follows. Flag-STING(1-160):

467 5’-CGCGGATCCATGCCCCACTCCAGCCTGCAT-3’,

468 5’-CCGGAATTCTGCCAGCCCATGGGCCACGTT-3’; Flag-STING(1-240):

469 5’-CGCGGATCCATGCCCCACTCCAGCCTGCAT-3’,

470 5’-CCGGAATTCGTAAACCCGATCCTTGATGCC-3; Flag-STING(41-379):

471 5’-CGCGGATCCATGGAGCACACTCTCCGGTAC-3’,

472 5’-CCGGAATTCTCAAGAGAAATCCGTGCGGAG-3’; Flag-STING(81-379):

473 5’-CGCGGATCCATGTACTGGAGGACTGTGCGG-3’,

474 5’-CCGGAATTCTCAAGAGAAATCCGTGCGGAG-3’; Flag-STING(111-379):

475 5’-CGCGGATCCATGGCGGTCGGCCCGCCCTTC-3’,

476 5’-CCGGAATTCTCAAGAGAAATCCGTGCGGAG-3’; Flag-STING(151-379):

477 5’-CGCGGATCCATGAATTTCAACGTGGCCCAT-3’,

478 5’-CCGGAATTCTCAAGAGAAATCCGTGCGGAG-3’, Flag-STING(211-379):

479 5’-CGCGGATCCATGCTGGATAAACTGCCCCAG-3’,

5'-CCGGAATTCTCAAGAGAAATCCGTGCGGAG-3'; HA-PYRIN:

5'-CCGGAATTCATGAAGATGGCAAGCACCCGC-3',

5'-CCGCTCGAGTAAACCCATCCACTCCTCTTC-3'; HA-NACHT:

5'-CCGGAATTCATGCTGGAGTACCTTTCGAGA-3', HA-LRR:

5'-ATCGAGCTCATGTCTCAGCAAATCAGGCTG-3',

5'-CCGCTCGAGCCAAGAAGGCTCAAAGACGAC-3'.

Lentivirus production and infection.

The targeting sequences of shRNAs for the human STING, NLRP3, ASC and Casp-1 were as follows: sh-STING: GCCCGGATTCGAACTTACAAT; sh-NLRP3: 5'-CAGGTTTGACTATCTGTTCT-3'; sh-ASC: 5'-GATGCGGAAGCTCTTCAGTTTCA-3'; sh-caspase-1: 5'-GTGAAGAGATCCTTCTGTA-3'. A PLKO.1 vector encoding shRNA for a negative control (Sigma-Aldrich, St. Louis, MO, USA) or a specific target molecule (Sigma-Aldrich) was transfected into HEK293T cells together with psPAX2 and pMD2.G with Lipofectamine 2000. Culture supernatants were harvested 36 and 60 h after transfection and then centrifuged at 2,200 rpm for 15 min. THP-1 cells were infected with the supernatants contain lentiviral particles in the presence of 4 μg/ml polybrene (Sigma). After 48 h of culture, cells were selected by 1.5 μg/ml puromycin (Sigma). Hela cells were selected by 2.5 μg/ml puromycin (Sigma). The results of each sh-RNA-targeted protein were detected by immunoblot analysis.

Enzyme-linked immunosorbent assay (ELISA)

Concentrations of human IL-1β in culture supernatants were measured by ELISA kit (BD

Biosciences, San Jose, CA, USA). The mouse IL-1β ELISA Kit was purchased from R&D.

Activated caspase-1 and mature IL-1β measurement

Supernatant of the cultured cells was collected for 1 ml in the cryogenic vials (Corning). The supernatant was centrifuged at 12,000 rpm for 10 min each time by Amicon Ultra (UFC500308) from Millipore for protein concentrate. The concentrated supernatant was mixed with SDS loading buffer for western blotting analysis with antibodies for detection of activated caspase-1 (D5782 1:500; Cell Signaling) or mature IL-1β (Asp116 1:500; Cell Signaling). Adherent cells in each well were lysed with the lyses buffer described below, followed by immunoblot analysis to determine the cellular content of various protein.

Western blot analysis

HEK293T whole-cell lysates were prepared by lysing cells with buffer (50 mM Tris-HCl, pH7.5, 300 mM NaCl, 1% Triton-X, 5 mM EDTA and 10% glycerol). The TPA-differentiated THP-1 cells lysates were prepared by lysing cells with buffer (50 mM Tris-HCl, pH7.5, 150 mM NaCl, 0.1% Nonidetp 40, 5 mM EDTA and 10% glycerol). Protein concentration was determined by Bradford assay (Bio-Rad, Hercules, CA, USA). Cultured cell lysates (30 μg) were electrophoresed in an 8-12% SDS-PAGE gel and transferred to a PVDF membrane (Millipore, MA, USA). PVDF membranes were blocked with 5% skim milk in phosphate buffered saline with 0.1% Tween 20 (PBST) before being incubated with the antibody. Protein band were detected using a Luminescent image Analyzer (Fujifilm LAS-4000).

524 **Co-immunoprecipitation assays**

525 HEK293T whole-cell lysates were prepared by lysing cells with buffer (50 mM Tris-HCl,
526 pH7.5, 300 mM NaCl, 1% Triton-X, 5 mM EDTA, and 10% glycerol). TPA-differentiated THP-1
527 cells lysates were prepared by lysing cells with buffer (50 mM Tris-HCl, pH7.5, 150 mM NaCl, 0.1%
528 Nonidetp40, 5 mM EDTA, and 10% glycerol). Lysates were immunoprecipitated with control
529 mouse immunoglobulin G (IgG) (Invitrogen) or anti-Flag antibody (Sigma, F3165) with Protein-G
530 Sepharose (GE Healthcare, Milwaukee, WI, USA).

531

532 **Confocal microscopy**

533 HEK293T cells and Hela cells were transfected with plasmids for 24–36 h. Cells were fixed
534 in 4% paraformaldehyde at room temperature for 15 min. After being washed three times with PBS,
535 permeabilized with PBS containing 0.1% Triton X-100 for 5 min, washed three times with PBS, and
536 finally blocked with PBS containing 5% BSA for 1 h. The cells were then incubated with the
537 monoclonal mouse anti-Flag antibody (F3165, Sigma) and Monoclonal rabbit anti-HA (H6908,
538 Sigma) overnight at 4°C, followed by incubation with FITC-conjugate donkey anti-mouse IgG
539 (Abbkine) and Dylight 649-conjugate donkey anti-rabbit IgG (Abbkine) for 1 h. After washing three
540 times, cells were incubated with DAPI solution for 5 min, and then washed three more times with
541 PBS. Finally, the cells were analyzed using a confocal laser scanning microscope (Fluo View
542 FV1000; Olympus, Tokyo, Japan).

543

544 **Real-time PCR**

545 Total RNA was extracted with TRIzol reagent (Invitrogen), following the manufacturer's

546 instructions. Real-time quantitative-PCR was performed using the Roche LC480 and SYBR
547 qRT-PCR kits (DBI Bio-science, Ludwigshafen, Germany) in a reaction mixture of 20 μl SYBR
548 Green PCR master mix, 1 μl DNA diluted template, and RNase-free water to complete the 20 μl
549 volume. Real-time PCR primers were designed by Primer Premier 5.0 and their sequences were as
550 follows: HSV-1 ICP27 forward, 5'-GCATCCTTCGTGTTTGTCATT-3', HSV-1 ICP27 reverse,
551 5'-GCATCTTCTCTCCGACCCCG-3'. HSV-1 UL30 forward,
552 5'-CATCACCGACCCGGAGAGGGAC-3', HSV-1 UL30 reverse,
553 5'-GGGCCAGGCGCTTGTTGGTGTA-3'. SeV P protein forward, 5'-
554 CAAAAGTGAGGGCGAAGGAGAA-3', SeV P protein reverse, 5'-
555 CGCCCAGATCCTGAGATACAGA-3'. ZIKV forward,
556 5'-GGTCAGCGTCCTCTCTAATAAACG-3', ZIKV reverse,
557 5'-GCACCCTAGTGTCCACTTTTTCC-3'. IL-1β forward,
558 5'-CACGATGCACCTGTACGATCA-3', IL-1β reverse, 5'-GTTGCTCCATATCCTGTCCCT-3'.
559 GAPDH forward, 5'-AAGGCTGTGGGCAAGG-3', GAPDH reverse,
560 5'-TGGAGGAGTGGGTGTCG-3'. Mouse GAPDH forward, 5'-TGGCCTTCCGTGTTCCTAC-3',
561 Mouse GAPDH reverse, 5'-GAGTTGCTGTTGAAGTCGCA-3'. Mouse IL-1β forward,
562 5'-GAAATGCCACCTTTTGACAGTG-3', Mouse IL-1β reverse,
563 5'-TGGATGCTCTCATCAGGACAG-3'. Mouse IL-6 forward,
564 5'-ACAAAGCCAGAGTCCTTCAGA -3', Mice IL-6 reverse,
565 5'-TCCTTAGCCACTCCTTCTGT-3'. Mice TNF-α forward,
566 5'-ACTGAACTTCGGGGTGATCG-3', Mice TNF-α reverse,
567 5'-TCTTTGAGATCCATGCCGTTG-3'.

568

569 **ASC oligomerization detection**

570 HEK293T cells were transfected with plasmids for 24–36 h. Cell lysates were centrifugated at
571 6000 rpm for 15 min. The supernatants of the lysates were mixed with SDS loading buffer for
572 western blot analysis with antibody against ASC. The pellets of the lysates were washed with PBS
573 for three times and cross-linked using fresh DSS (2 mM, Sigma) at 37°C for 30 min. The
574 cross-linked pellets were then spanned down and the supernatant was mixed with SDS loading
575 buffer for western blotting analysis.

576

577 **Statistical analyses**

578 All experiments were reproducible and repeated at least three times with similar results.
579 Parallel samples were analyzed for normal distribution using Kolmogorov-Smirnov tests. Abnormal
580 values were eliminated using a follow-up Grubbs test. Levene's test for equality of variances was
581 performed, which provided information for Student's t-tests to distinguish the equality of means.
582 Means were illustrated using histograms with error bars representing the SD; a P value of <0.05 was
583 considered statistically significant.

584

585

Acknowledgments

We thank Dr. Di Wang of Zhejiang University School of Medicine, China for kindly providing C57BL/6 NLRP3$^{-/-}$ mice, Dr. Jun Cui of Sun Yat-Sen University, Guangzhou 510275, China for Human acute monocytic leukemia (THP-1) cells, and Dr. Bo Zhong of Wuhan University, China, for kindly providing Herpes simplex virus 1 strain, Sendai virus strain, and plasmids encoding ubiquitin and mutants.

This work was supported by National Natural Science Foundation of China (81730061 and 81471942), Postdoctoral Science Foundation of China (2018T110923), National Health and Family Planning Commission of China (National Mega Project on Major Infectious Disease Prevention) (2017ZX10103005 and 2017ZX10202201), and Guangdong Province "Pearl River Talent Plan" Innovation and Entrepreneurship Team Project (2017ZT07Y580).

Author contributions:

W.W., D.H., Y.F., Q.Z., W.L., F.L., K.W., G.L., Y.L., and J.W. contributed the conceptualization. W.W., D.H., Y.F., C.W., A.L., Y.W., K.C., M.T., F.X., Q.Z., M.A.S., W.C., P.P., P.W., and W.L. contributed the methodology, conduction of experiments, and investigation. W.W., F.L., K.W., G.L., Y.L., and J.W. contributed the reagents and resources. W.W., and J.W. contributed the writing the original draft of the paper. W.W., and J.W. contributed the review and editing the paper. F.L., K.W., G.L., and Y.L. contributed the visualization or funding acquisition. J.W. contributed the supervision and funding acquisition.

Conflict of Interests: The authors have no conflict of interests.

608 **References**

609

610 Abe T, Barber GN (2014) Cytosolic-DNA-mediated, STING-dependent proinflammatory gene
611 induction necessitates canonical NF-kappaB activation through TBK1. *J Virol* 88: 5328-5341

612 Abe T, Harashima A, Xia T, Konno H, Konno K, Morales A, Ahn J, Gutman D, Barber GN (2013)
613 STING recognition of cytoplasmic DNA instigates cellular defense. *Mol Cell* 50: 5-15

614 Akira S, Uematsu S, Takeuchi O (2006) Pathogen recognition and innate immunity. *Cell* 124:
615 783-801

616 Barry R, John SW, Liccardi G, Tenev T, Jaco I, Chen CH, Choi J, Kasperkiewicz P,
617 Fernandes-Alnemri T, Alnemri E, Drag M, Chen Y, Meier P (2018) SUMO-mediated regulation
618 of NLRP3 modulates inflammasome activity. *Nat Commun* 9: 3001

619 Chen J, Chen ZJ (2018) PtdIns4P on dispersed trans-Golgi network mediates NLRP3 inflammasome
620 activation. *Nature* 564: 71-76

621 Chen Q, Sun L, Chen ZJ (2016) Regulation and function of the cGAS-STING pathway of cytosolic
622 DNA sensing. *Nat Immunol* 17: 1142-1149

623 Compan V, Baroja-Mazo A, Lopez-Castejon G, Gomez AI, Martinez CM, Angosto D, Montero MT,
624 Herranz AS, Bazan E, Reimers D, Mulero V, Pelegrin P (2012) Cell volume regulation
625 modulates NLRP3 inflammasome activation. *Immunity* 37: 487-500

626 Dinarello CA (2009) Immunological and inflammatory functions of the interleukin-1 family. *Annu*
627 *Rev Immunol* 27: 519-550

628 Gaidt MM, Ebert TS, Chauhan D, Ramshorn K, Pinci F, Zuber S, O'Duill F, Schmid-Burgk JL, Hoss
629 F, Buhmann R, Wittmann G, Latz E, Subklewe M, Hornung V (2017) The DNA inflammasome

630 in human myeloid cells is initiated by a STING-cell death program upstream of NLRP3. *Cell*
631 171: 1110-1124

632 Guo C, Chi Z, Jiang D, Xu T, Yu W, Wang Z, Chen S, Zhang L, Liu Q, Guo X, Zhang X, Li W, Lu
633 L, Wu Y, Song BL, Wang D (2018) Cholesterol homeostatic regulator SCAP-SREBP2
634 integrates NLRP3 inflammasome activation and cholesterol biosynthetic signaling in
635 macrophages. *Immunity* 49: 842-856

636 Halle A, Hornung V, Petzold GC, Stewart CR, Monks BG, Reinheckel T, Fitzgerald KA, Latz E,
637 Moore KJ, Golenbock DT (2008) The NALP3 inflammasome is involved in the innate immune
638 response to amyloid-beta. *Nat Immunol* 9: 857-865

639 Hardison SE, Brown GD (2012) C-type lectin receptors orchestrate antifungal immunity. *Nat*
640 *Immunol* 13: 817-822

641 Hottz ED, Lopes JF, Freitas C, Valls-de-Souza R, Oliveira MF, Bozza MT, Da PA, Weyrich AS,
642 Zimmerman GA, Bozza FA, Bozza PT (2013) Platelets mediate increased endothelium
643 permeability in dengue through NLRP3-inflammasome activation. *Blood* 122: 3405-3414

644 Humphries F, Bergin R, Jackson R, Delagic N, Wang B, Yang S, Dubois AV, Ingram RJ, Moynagh
645 PN (2018) The E3 ubiquitin ligase Pellino2 mediates priming of the NLRP3 inflammasome. *Nat*
646 *Commun* 9: 1560

647 Ishikawa H, Barber GN (2008) STING is an endoplasmic reticulum adaptor that facilitates innate
648 immune signalling. *Nature* 455: 674-678

649 Ishikawa H, Ma Z, Barber GN (2009) STING regulates intracellular DNA-mediated, type I
650 interferon-dependent innate immunity. *Nature* 461: 788-792

651 Johnson KE, Chikoti L, Chandran B (2013) Herpes simplex virus 1 infection induces activation and

652 subsequent inhibition of the IFI16 and NLRP3 inflammasomes. *J Virol* 87: 5005-5018

653 Juliana C, Fernandes-Alnemri T, Kang S, Farias A, Qin F, Alnemri ES (2012) Non-transcriptional
654 priming and deubiquitination regulate NLRP3 inflammasome activation. *J Biol Chem* 287:
655 36617-36622

656 Kanneganti TD, Body-Malapel M, Amer A, Park JH, Whitfield J, Franchi L, Taraporewala ZF,
657 Miller D, Patton JT, Inohara N, Nunez G (2006) Critical role for Cryopyrin/Nalp3 in activation
658 of caspase-1 in response to viral infection and double-stranded RNA. *J Biol Chem* 281:
659 36560-36568

660 Komune N, Ichinohe T, Ito M, Yanagi Y (2011) Measles virus V protein inhibits NLRP3
661 inflammasome-mediated interleukin-1beta secretion. *J Virol* 85: 13019-13026

662 Lawrence TM, Hudacek AW, de Zoete MR, Flavell RA, Schnell MJ (2013) Rabies virus is
663 recognized by the NLRP3 inflammasome and activates interleukin-1beta release in murine
664 dendritic cells. *J Virol* 87: 5848-5857

665 Martinon F, Agostini L, Meylan E, Tschopp J (2004) Identification of bacterial muramyl dipeptide as
666 activator of the NALP3/cryopyrin inflammasome. *Curr Biol* 14: 1929-1934

667 Martinon F, Mayor A, Tschopp J (2009) The inflammasomes: guardians of the body. *Annu Rev*
668 *Immunol* 27: 229-265

669 Martinon F, Petrilli V, Mayor A, Tardivel A, Tschopp J (2006) Gout-associated uric acid crystals
670 activate the NALP3 inflammasome. *Nature* 440: 237-241

671 Maruzuru Y, Ichinohe T, Sato R, Miyake K, Okano T, Suzuki T, Koshiba T, Koyanagi N, Tsuda S,
672 Watanabe M, Arii J, Kato A, Kawaguchi Y (2018) Herpes simplex virus 1 VP22 inhibits
673 AIM2-dependent inflammasome activation to enable efficient viral replication. *Cell Host*

Microbe 23: 254-265

Muruve DA, Petrilli V, Zaiss AK, White LR, Clark SA, Ross PJ, Parks RJ, Tschopp J (2008) The inflammasome recognizes cytosolic microbial and host DNA and triggers an innate immune response. *Nature* 452: 103-107

Negash AA, Ramos HJ, Crochet N, Lau DT, Doehle B, Papic N, Delker DA, Jo J, Bertoletti A, Hagedorn CH, Gale MJ (2013) IL-1beta production through the NLRP3 inflammasome by hepatic macrophages links hepatitis C virus infection with liver inflammation and disease. *PLoS Pathog* 9: e1003330

Py BF, Kim MS, Vakifahmetoglu-Norberg H, Yuan J (2013) Deubiquitination of NLRP3 by BRCC3 critically regulates inflammasome activity. *Mol Cell* 49: 331-338

Rajan JV, Rodriguez D, Miao EA, Aderem A (2011) The NLRP3 inflammasome detects encephalomyocarditis virus and vesicular stomatitis virus infection. *J Virol* 85: 4167-4172

Ramos HJ, Lanteri MC, Blahnik G, Negash A, Suthar MS, Brassil MM, Sodhi K, Treuting PM, Busch MP, Norris PJ, Gale MJ (2012) IL-1beta signaling promotes CNS-intrinsic immune control of West Nile virus infection. *PLoS Pathog* 8: e1003039

Roizman, B., Knipe, D.M., and Whitley, R.J. (2013) Herpes simplex viruses. In *Fields Virology*. Knipe, D. M. (ed) pp 1823–1897. Lippincott-Williams &Wilkins Press.

Schroder K, Tschopp J (2010) The inflammasomes. *Cell* 140: 821-832

Schroder K, Zhou R, Tschopp J (2010) The NLRP3 inflammasome: a sensor for metabolic danger? *Science* 327: 296-300

Shenoy AR, Wellington DA, Kumar P, Kassa H, Booth CJ, Cresswell P, MacMicking JD (2012) GBP5 promotes NLRP3 inflammasome assembly and immunity in mammals. *Science* 336:

481-485

Song H, Liu B, Huai W, Yu Z, Wang W, Zhao J, Han L, Jiang G, Zhang L, Gao C, Zhao W (2016) The E3 ubiquitin ligase TRIM31 attenuates NLRP3 inflammasome activation by promoting proteasomal degradation of NLRP3. *Nat Commun* 7: 13727

Song N, Li T (2018) Regulation of NLRP3 Inflammasome by Phosphorylation. *Front Immunol* 9: 2305

Subramanian N, Natarajan K, Clatworthy MR, Wang Z, Germain RN (2013) The adaptor MAVS promotes NLRP3 mitochondrial localization and inflammasome activation. *Cell* 153: 348-361

Swanson KV, Junkins RD, Kurkjian CJ, Holley-Guthrie E, Pendse AA, El MR, Petrucelli A, Barber GN, Benedict CA, Ting JP (2017) A noncanonical function of cGAMP in inflammasome priming and activation. *J Exp Med* 214: 3611-3626

Takeuchi O, Akira S (2010) Pattern recognition receptors and inflammation. *Cell* 140: 805-820

Ting JP, Lovering RC, Alnemri ES, Bertin J, Boss JM, Davis BK, Flavell RA, Girardin SE, Godzik A, Harton JA, Hoffman HM, Hugot JP, Inohara N, Mackenzie A, Maltais LJ, Nunez G, Ogura Y, Otten LA, Philpott D, Reed JCet al (2008) The NLR gene family: a standard nomenclature. *Immunity* 28: 285-287

Wang H, Lei X, Xiao X, Yang C, Lu W, Huang Z, Leng Q, Jin Q, He B, Meng G, Wang J (2015) Reciprocal Regulation between Enterovirus 71 and the NLRP3 Inflammasome. *Cell Rep* 12: 42-48

Wang W, Li G, De Wu, Luo Z, Pan P, Tian M, Wang Y, Xiao F, Li A, Wu K, Liu X, Rao L, Liu F, Liu Y, Wu J (2018) Zika virus infection induces host inflammatory responses by facilitating NLRP3 inflammasome assembly and interleukin-1beta secretion. *Nat Commun* 9: 106

718 Wang W, Xiao F, Wan P, Pan P, Zhang Y, Liu F, Wu K, Liu Y, Wu J (2017) EV71 3D Protein binds
719 with NLRP3 and enhances the assembly of inflammasome complex. *PLoS Pathog* 13:
720 e1006123
721 Webster SJ, Brode S, Ellis L, Fitzmaurice TJ, Elder MJ, Gekara NO, Tourlomousis P, Bryant C,
722 Clare S, Chee R, Gaston H, Goodall JC (2017) Detection of a microbial metabolite by STING
723 regulates inflammasome activation in response to Chlamydia trachomatis infection. *PLoS*
724 *Pathog* 13: e1006383
725 Wu J, Sun L, Chen X, Du F, Shi H, Chen C, Chen ZJ (2013) Cyclic GMP-AMP is an endogenous
726 second messenger in innate immune signaling by cytosolic DNA. *Science* 339: 826-830
727 Yan Y, Jiang W, Liu L, Wang X, Ding C, Tian Z, Zhou R (2015) Dopamine controls systemic
728 inflammation through inhibition of NLRP3 inflammasome. *Cell* 160: 62-73
729 Ye Z, Ting JP (2008) NLR, the nucleotide-binding domain leucine-rich repeat containing gene
730 family. *Curr Opin Immunol* 20: 3-9
731 Yoneyama M, Kikuchi M, Natsukawa T, Shinobu N, Imaizumi T, Miyagishi M, Taira K, Akira S,
732 Fujita T (2004) The RNA helicase RIG-I has an essential function in double-stranded
733 RNA-induced innate antiviral responses. *Nat Immunol* 5: 730-737
734
735
736

737 **Figure Legends**

738

739 **Figure 1 – STING interacts with NLRP3 to facilitate the inflammasome activation.**

740 **A**–**C** HEK293T cells were co-transfected with pFlag-STING and pHA-NLRP3 (A and B), or with

741 pFlag-STING, pHA-NLRP3, pHA-ASC, and pHA-Casp-1 (C).

742 **D** Diagrams of NLRP3, PYRIN, NACHT, and LRR.

743 **E**, **F** HEK293T cells were co-transfected with pHA-STING and pFlag-NLRP3, pFlag-PYRIN,

744 pFlag-NACHT, or pFlag-LRR (E), or with pFlag-STING and pHA-NLRP3, pHA-PYRIN,

745 pHA-NACHT, or pHA-LRR (F).

746 **G** Diagrams of STING and its truncated proteins.

747 **H** HEK293T cells were co-transfected with pHA-NLRP3 and pFlag-STING or truncated proteins.

748 **I** HEK293T cells were co-transfected with plasmids encoding NLRP3, ASC, pro-Casp-1, and

749 pro-IL-1β to generate a pro-IL-1β cleavage system (NACI), and transfected with pFlag-STING or

750 truncated proteins. IL-1β in supernatants was determined by ELISA.

751 **J** HEK293T cells were co-transfected with pFlag-ASC, pHA-NLRP3, or pFlag-STING.

752 **A**–**C**, **E**, **F**, **H** and **J** Cell lysates were subjected to co-immunoprecipitation (Co-IP) using IgG

753 (Mouse) and anti-Flag antibody (A, F), IgG (Rabbit) and anti-HA antibody (B, J), anti-HA antibody

754 (C), and anti-Flag antibody (E, H), and analyzed by immunoblotting using anti-HA or anti-Flag

755 antibody (top) or subjected directly to Western blot using anti-Flag or anti-HA antibody (input)

756 (bottom).

757 **K** HEK293T cells were co-transfected with pFlag-ASC, pHA-NLRP3, and pMyc-STING. Pellets

758 were subjected to ASC oligomerization assays (top) and lysates were prepared for Western blots

(bottom).

L, **M** HEK293T cells (L) or Hela cells (M) were co-transfected with pFlag-STING and/or pHA-NLRP3. Sub-cellular localization of Flag-STING (green), HA-NLRP3 (red), and DAPI (blue) were examined by confocal microscopy.

Data shown are means ± SEMs; $^{**}p < 0.01$, ***$p < 0.0001$; ns, no significance.

Figure 2 – HSV-1 infection promotes the STING-NLRP3 interaction.

A, **B** TPA-differentiated THP-1 macrophages were mock-infected or infected with HSV-1 (MOI=1) for 4 h.

C, **D** HEK293T cells (C) and Hela cells (D) were co-transfected with pFlag-STING and pHA-NLRP3, and then infected with HSV-1 (MOI=1) for 2–4 h.

E TPA-differentiated THP-1 macrophages were transfected with HSV120 (3 μg/ml) by Lipo2000 for 4 h.

F, **G** HEK293T cells (F) and Hela cells (G) were co-transfected with pFlag-STING and pHA-NLRP3 and then transfected with HSV120 (3 μg/ml) for 4 h.

H Primary MEFs were primed with LPS (1 μg/ml) for 6 h, and then infected with HSV-1 (MOI=1) for 4 h or transfected with HSV120 (3 μg/ml) for 4 h.

A–**H** Cell lysates were subjected to Co-IP using IgG (Mouse) or anti-NLRP3 antibody (A), anti-STING antibody (B), IgG (Mouse) or anti-Flag antibody (C), anti-Flag antibody (D), IgG (Mouse) or anti-NLRP3 antibody (E), IgG (Mouse) or anti-Flag antibody (F), anti-Flag antibody (G), and IgG (Mouse) or anti-NLRP3 antibody (H), and then analyzed by immunoblotting using anti-NLRP3 and anti-STING antibody (top) or analyzed directly by immunoblotting using

781 anti-NLRP3 and anti-STING antibody (as input) (bottom).

782

783 **Figure 3 – HSV-1 infection induces IL-1β expression and secretion.**

784 **A**–**K** TPA-differentiated THP-1 macrophages were treated with 2 μM Nigericin for 2 h, and infected
785 with HSV-1 at MOI=0.1, 0.2, 0.4, and 0.8 for 8 h (A, C, E and G), infected with HSV-1 at MOI=0.8
786 for 2, 4, 6, and 8 h (B, D, F and H), or transfected with HSV120 (3 μg/ml) for 2, 4, and 6 h (I–K).
787 **L**–**O** Mice primary MEFs were primed with LPS (1 μg/ml) for 6 h, and then treated with 5 mM ATP
788 for 2 h or infected with HSV-1 (MOI=1) (L and N) or transfected with HSV120 (3 μg/ml) (M, O)
789 for 2, 4, and 6 h.

790 **A**, **B**, **I**, **L** and **M** IL-1β protein was determined by ELISA.

791 **C**, **D** and **J** Matured IL-1β (p17) and cleaved Casp-1 in supernatants (top) and pro-IL-1β production
792 in lysates (bottom) were determined by Western-blot analyses.

793 **E**, **F**, **G**, **H**, **K**, **N** and **O** IL-1β mRNA and GAPDH mRNA (E, F), HSV-1 ICP27 mRNA and
794 GAPDH mRNA (G, H and N), and IFN-β mRNA and GAPDH mRNA (K, O) were quantified by
795 RT-PCR.

796 Data shown are means ± SEMs; *$p < 0.05$, **$p < 0.01$, ***$p < 0.0001$; ns, no significance.

797

798 **Figure 4 – The NLRP3 inflammasome is required for HSV-1-induced IL-1β activation.**

799 **A**–**F** TPA-differentiated THP-1 macrophages were treated with 2 μM Nigericin for 2 h, infected
800 with HSV-1 at MOI=0.8 for 8 h, and then treated with Glybenclamide (25 μg/ml) (A, B and E) or
801 Ac-YVAD-cmk (10 μg/ml) (C, D and F).

802 **G**–**K** THP-1 cells stably expressing shRNAs targeting NLRP3, ASC or Casp-1 were generated and

803 then treated with 2 μM Nigericin for 2 h (G, H) or infected with HSV-1 at MOI=0.8 for 8 h (I–K).
804 **L–N** Primary MEFs of C57BL/6 WT mice and C57BL/6 NLRP3$^{-/-}$ mice were primed with LPS (1
805 μg/ml) for 6 h, and then treated with 5 mM ATP for 2 h or infected with HSV-1 (MOI=1) for 6 h.
806 NLRP3 and GAPDH protein in lysates were determined by Western blot (L). IL-1β levels were
807 determined by ELISA (A, C, G and M). Matured IL-1β (p17) and cleaved Casp-1 (p22/p20) in
808 supernatants (top) or pro-IL-1β and pro-Casp-1 in lysates (bottom) were determined by Western-blot
809 (B, H and J). HSV-1 ICP27 mRNA and GAPDH mRNA were quantified by RT-PCR (E, F, K and N).
810 Data shown are means ± SEMs; ***$p < 0.0001$; ns, no significance.
811
812 **Figure 5 – STING recruits NLRP3 to the ER and promotes the inflammasome formation.**
813 **A–D** Hela cells were co-transfected with pFlag-STING and pHA-NLRP3 (A), transfected with
814 pFlag-NLRP3 and infected with HSV-1 (MOI=1) for 4 h or transfected with HSV120 (3 μg/ml) for
815 4 h (B, C and D). Sub-cellular localization of HA-NLRP3 (green) (A), Flag-STING (red) (A), ER
816 Blue (blue) (A, D), Flag-NLRP3 (red) (B, C), Calnexin (green) (B), DAPI (blue) (B and C),
817 Calnexin (green) (C) and HA-NLRP3 (red) (D) were examined by confocal microscopy.
818 **E–G** Hela cells were co-transfected with pFlag-STING and pHA-NLRP3 (E). THP-1 macrophages
819 were infected with HSV-1 (MOI=1) for 4 h (F). Mice primary MEFs were primed with LPS (1
820 μg/ml) for 6 h and infected with HSV-1 (MOI=1) for 4 h (G). Flag-NLRP3, HA-STING, Calnexin,
821 and GAPDH in whole cell lysate (WCL) and purified ER were determined by Western-blot
822 analyses.
823 **H**, **I** Hela cells stably expressing sh-STNG were transfected with pFlag-NLRP3 and infected with
824 HSV-1 (MOI=1) for 4 h or transfected with HSV120 (3 μg/ml) for 4 h. Sub-cellular localization of

825 Flag-NLRP3 (red) (H), Calnexin (green) (H), DAPI (blue) (H), HA-NLRP3 (red) (I) and ER blue (I)
826 were examined by confocal microscopy.
827 **J–L** Hela cells stably expressing sh-STING were transfected with pHA-NLRP3 and infected with
828 HSV-1 (MOI=1) for 4 h (J). THP-1 cells stably expressing sh-STING were differentiated to
829 macrophages, and infected with HSV-1 (MOI=1) for 4 h (K). Primary MEFs stably expressing
830 sh-STING were primed with LPS (1 μg/ml) for 6 h, and infected with HSV-1 (MOI=1) for 4 h (L).
831 HA-NLRP3 (J), NLRP3 (K, I), STING (J–L), Calnexin (ER) (J–L), and GAPDH (J–L) in WCL and
832 purified ER fraction were determined by Western-blot analyses.
833
834 **Figure 6 – STING deubiquitinates NLRP3 to activate the NLRP3 inflammasome.**
835 **A–E** Hela cells were co-transfected with pFlag-NLRP3, pHA-Ubiquitin, and pMyc-STING (A),
836 with pFlag-NLRP3, pHA-Ubiquitin, pHA-Ubiquitin mutations (K48R), pHA-Ubiquitin mutations
837 (K63R) and pMyc-STING (B), with pFlag-NLRP3, pHA-Ubiquitin, pHA-Ubiquitin
838 mutations(K48O), pHA-Ubiquitin mutations(K63O), and pMyc-STING (C), with pFlag-NLRP3 and
839 pHA-Ubiquitin and then infected with HSV-1(MOI=1) for 2 and 4 h (D), and transfected with
840 HSV120 (3 μg/ml) for 2 and 4 h (E). Cell lysates were prepared and subjected to denature-IP using
841 anti-Flag antibody and then analyzed by immunoblotting using an anti-HA or anti-Flag antibody
842 (top) or subjected directly to Western blot using an anti-Flag, anti-HA or anti-Myc antibody (as
843 input) (bottom).
844 **F–I** TPA-differentiated THP-1 macrophages were infected with HSV-1 (MOI=1) for 2 and 4 h (F),
845 and transfected with HSV120 (3 μg/ml) for 2, 4 and 6 h (G). Mice primary MEFs were infected
846 with HSV-1 (MOI=1) for 2 h (H). THP-1 cells stably expressing sh-NC or sh-STING were

generated and differentiated to macrophages and then infected with HSV-1 (MOI=1) for 4 h (I). Cell lysates were prepared and subjected to denature-IP using anti-NLRP3 antibody and then analyzed by immunoblotting using an anti-Ubiquitin, anti-K48-Ubiquitin, anti-K63-Ubiquitin or anti-NLRP3 antibody (top) (F) or using anti-NLRP3 antibody (G, H and I), or subjected directly to Western blot using an anti- Ubiquitin or anti-NLRP3 antibody (as input) (bottom).

Figure 7 – STING is required for the NLRP3 inflammasome activation upon DNA virus infection.

A–**H** THP-1 cells stably expressing sh-NC or sh-STING were generated and differentiated to macrophages, and then infected with HSV-1 at MOI=0.8 for 2, 4, and 8 h (A–C), transfected with DNA90 (3 μg/ml), HSV120 (3 μg/ml) or infected with HSV-1 at MOI=0.8 for 8 h (D, E), and treated with 2 μM Nigericin for 2 h and infected with HSV-1 at MOI=0.8 for 8 h (F–H). IL-1β levels were determined by ELISA (A, D and F). Matured IL-1β (p17) and cleaved Casp-1 (p22/p20) in supernatants or STING, pro-IL-1β and pro-Casp-1 in lysates were determined by Western-blot (B, C and G). HSV-1 ICP27 mRNA and GAPDH mRNA were quantified by RT-PCR (C, H).

I–**M** THP-1 cells stably expressing shRNA targeting STING was generated and differentiated to macrophages, then infected with SeV (MOI=1) for 24 h, ZIKV (MOI=1) for 24 h or HSV-1 (MOI=0.8) for 8 h. IL-1β levels were determined by ELISA (I). Matured IL-1β (p17) and cleaved Casp-1 (p22/p20) in supernatants or STING, pro-IL-1β and pro-Casp-1 in lysates were determined by Western-blot (J). SeV P mRNA (K), ZIKV mRNA (L), HSV-1 ICP27 mRNA (M) and GAPDH mRNA were quantified by RT-PCR.

Data shown are means ± SEMs; *$p < 0.05$, **$p < 0.01$, ***$p < 0.0001$; ns, no significance.

Figure 8 – NLRP3 is critical for host defense against HSV-1 infection in mice.

A, **B** C57BL/6 WT mice (8-week-old, female, n=9) and C57BL/6 NLRP3$^{-/-}$ mice (8-week-old, female, n=5) were infected i.p. with HSV-1 at 1×10^7 pfu for 11 days. The survival rates (A) and body weights (B) of mice were evaluated.

C–**G** WT mice (8-week-old, female) and NLRP3$^{-/-}$ mice (8-week-old, female) were mock-infected i.p. with PBS (WT and NLRP3$^{-/-}$ mice, n=3) or infected i.p. with HSV-1 (WT mice, n=4, NLRP3$^{-/-}$ mice, n=3) at 1×10^7 pfu for 6 h. IL-1β in mice sera was determined by ELISA (C). IL-1β mRNA (D), IL-6 mRNA (E), TNF-α mRNA (F), HSV-1 UL30 mRNA (G) and GAPDH mRNA in mice blood were quantified by RT-PCR.

H–**J** WT mice (8-week-old, female, n=4) and NLRP3$^{-/-}$ mice (8-week-old, female, n=4) were infected i.p. with HSV-1 at 1×10^7 pfu for 1 days. IL-1β mRNA (H), IL-6 mRNA (I), and GAPDH mRNA in mice lung were quantified by RT-PCR. HSV-1 viral titers were measured by plaque assays for mice lung (J).

K–**M** WT mice (8-week-old, female, n=7) and NLRP3$^{-/-}$ mice (8-week-old, female, n=7) were infected i.p. with HSV-1 at 1×10^7 pfu for 4 days. IL-1β mRNA (K), IL-6 mRNA (L) and GAPDH mRNA in mice brain were quantified by RT-PCR. HSV-1 viral titers were measured by plaque assays for mice brain (M).

N, **O** WT mice (8-week-old, female) and NLRP3$^{-/-}$ mice (8-week-old, female) were infected i.p. with HSV-1 at 1×10^7 pfu for 1 day. The lung tissue (N) and brain tissue (O) were stained with histological analysis (H&E or IL-1β).

Data shown are means ± SEMs; *$p < 0.05$, **$p < 0.01$, ***$p < 0.0001$; ns, no significance.

Fig. 9. A proposed model for the regulation of NLRP3 inflammasome activation mediated by the cGAS-STING-NLRP3 pathway.

In resting cells and under normal physiological conditions, CUL1 interacts with NLRP3 to disrupt the inflammasome assembly, and catalyzes NLRP3 ubiquitination to repress the inflammasome activation (left). However, in response to inflammatory stimuli, CUL1 disassociates from NLRP3 to release the repression of inflammasome assembly and activation (right).

Figure 1

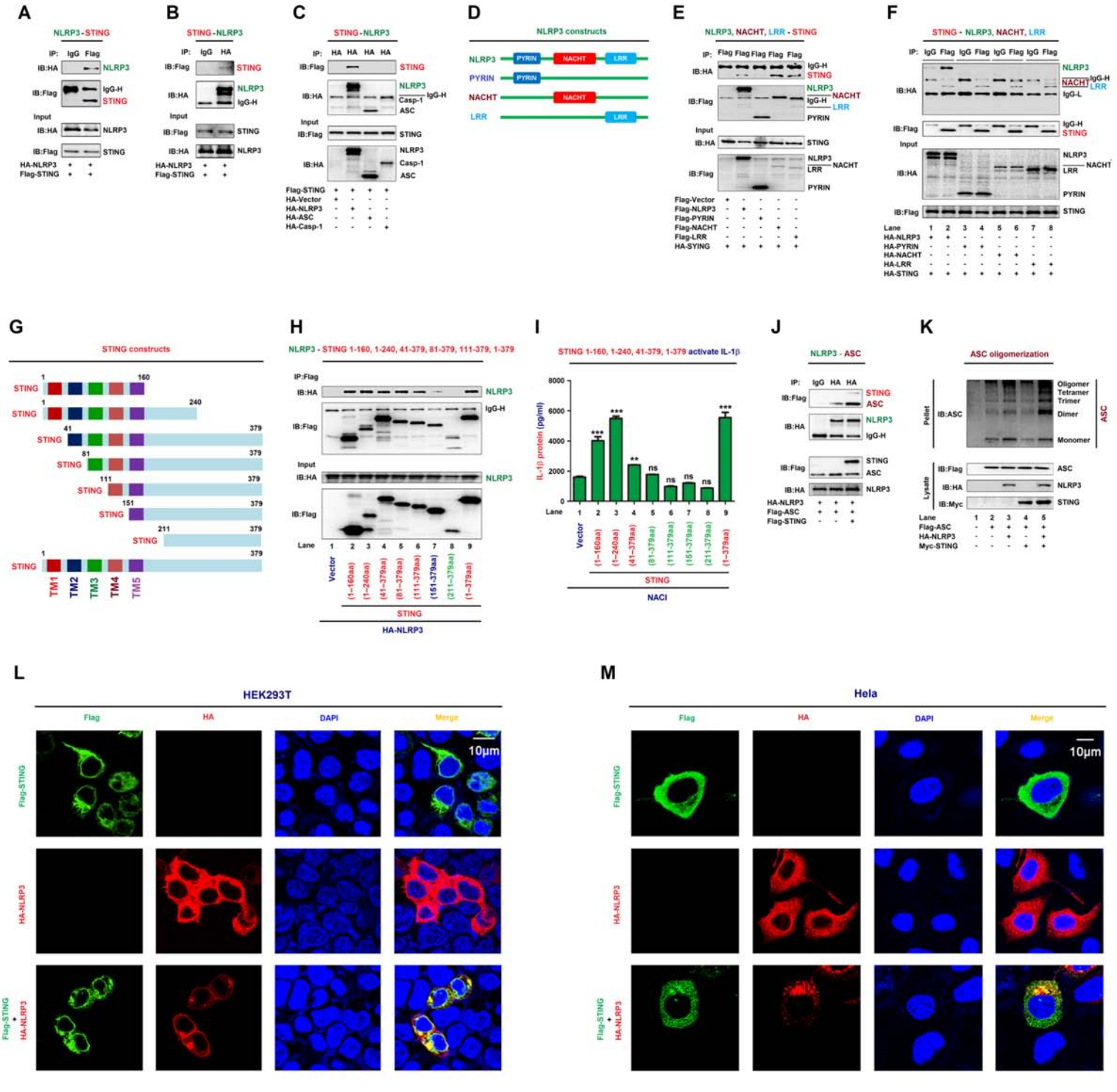
A
NLRP3 - STING
IP: IgG Flag
IB:HA
NLRP3
IB:Flag
IgG-H
STING
Input
IB:HA
NLRP3
IB:Flag
STING
HA-NLRP3 + +
Flag-STING + +
B
STING - NLRP3
IP: IgG HA
IB:Flag
STING
IB:HA
NLRP3
IgG-H
Input
IB:Flag
STING
IB:HA
NLRP3
HA-NLRP3 + +
Flag-STING + +
C
STING - NLRP3
IP: HA HA HA HA
IB:Flag
STING
IB:HA
NLRP3
Casp-1
IgG-H
ASC
Input
IB:Flag
STING
IB:HA
NLRP3
Casp-1
ASC
Flag-STING + + + +
HA-Vector + - - -
HA-NLRP3 - + - -
HA-ASC - - + -
HA-Casp-1 - - - +
D
NLRP3 constructs
NLRP3
PYRIN
NACHT
LRR
PYRIN
PYRIN
NACHT
NACHT
LRR
LRR
E
NLRP3, NACHT, LRR - STING
IP: Flag Flag Flag Flag Flag
IB:HA
IgG-H
STING
IB:Flag
NLRP3
IgG-H
NACHT
LRR
PYRIN
Input
IB:HA
STING
IB:Flag
NLRP3
LRR
NACHT
PYRIN
Flag-Vector + - - - -
Flag-NLRP3 - + - - -
Flag-PYRIN - - + - -
Flag-NACHT - - - + -
Flag-LRR - - - - +
HA-SYING + + + + +
F
STING - NLRP3, NACHT, LRR
IP: IgG Flag IgG Flag IgG Flag IgG Flag
IB:HA
NLRP3
NACHT
IgG-H
LRR
IgG-L
IB:Flag
IgG-H
STING
Input
IB:HA
NLRP3
LRR
NACHT
PYRIN
IB:Flag
STING
Lane 1 2 3 4 5 6 7 8
HA-NLRP3 + + - - - - - -
HA-PYRIN - - + + - - - -
HA-NACHT - - - - + + - -
HA-LRR - - - - - - + +
HA-STING + + + + + + + +
G
STING constructs
STING
TM1
TM2
TM3
TM4
TM5
H
NLRP3 - STING 1-160, 1-240, 41-379, 81-379, 111-379, 1-379
IP:Flag
IB:HA
NLRP3
IgG-H
IB:Flag
Input
IB:HA
NLRP3
IB:Flag
Lane 1 2 3 4 5 6 7 8 9
Vector
(1–160aa)
(1–240aa)
(41–379aa)
(81–379aa)
(111–379aa)
(151–379aa)
(211–379aa)
(1–379aa)
STING
HA-NLRP3
I
STING 1-160, 1-240, 41-379, 1-379 activate IL-1β
IL-1β protein (pg/ml)
8000
6000
4000
2000
0
***
***
**
ns
ns
ns
ns
***
Lane 1 2 3 4 5 6 7 8 9
Vector
(1–160aa)
(1–240aa)
(41–379aa)
(81–379aa)
(111–379aa)
(151–379aa)
(211–379aa)
(1–379aa)
STING
NACI
J
NLRP3 - ASC
IP: IgG HA HA
IB:Flag
STING
ASC
IB:HA
NLRP3
IgG-H
IB:Flag
STING
ASC
IB:HA
NLRP3
HA-NLRP3 + + +
Flag-ASC + + +
Flag-STING - - +
K
ASC oligomerization
Pellet
IB:ASC
Oligomer
Tetramer
Trimer
Dimer
Monomer
ASC
Lysate
IB:Flag
ASC
IB:HA
NLRP3
IB:Myc
STING
Lane 1 2 3 4 5
Flag-ASC - + + + +
HA-NLRP3 - - + - +
Myc-STING - - - + +
L
HEK293T
Flag
HA
DAPI
Merge
10μm
Flag-STING
HA-NLRP3
Flag-STING + HA-NLRP3
M
Hela
Flag
HA
DAPI
Merge
10μm
Flag-STING
HA-NLRP3
Flag-STING + HA-NLRP3

Figure 2

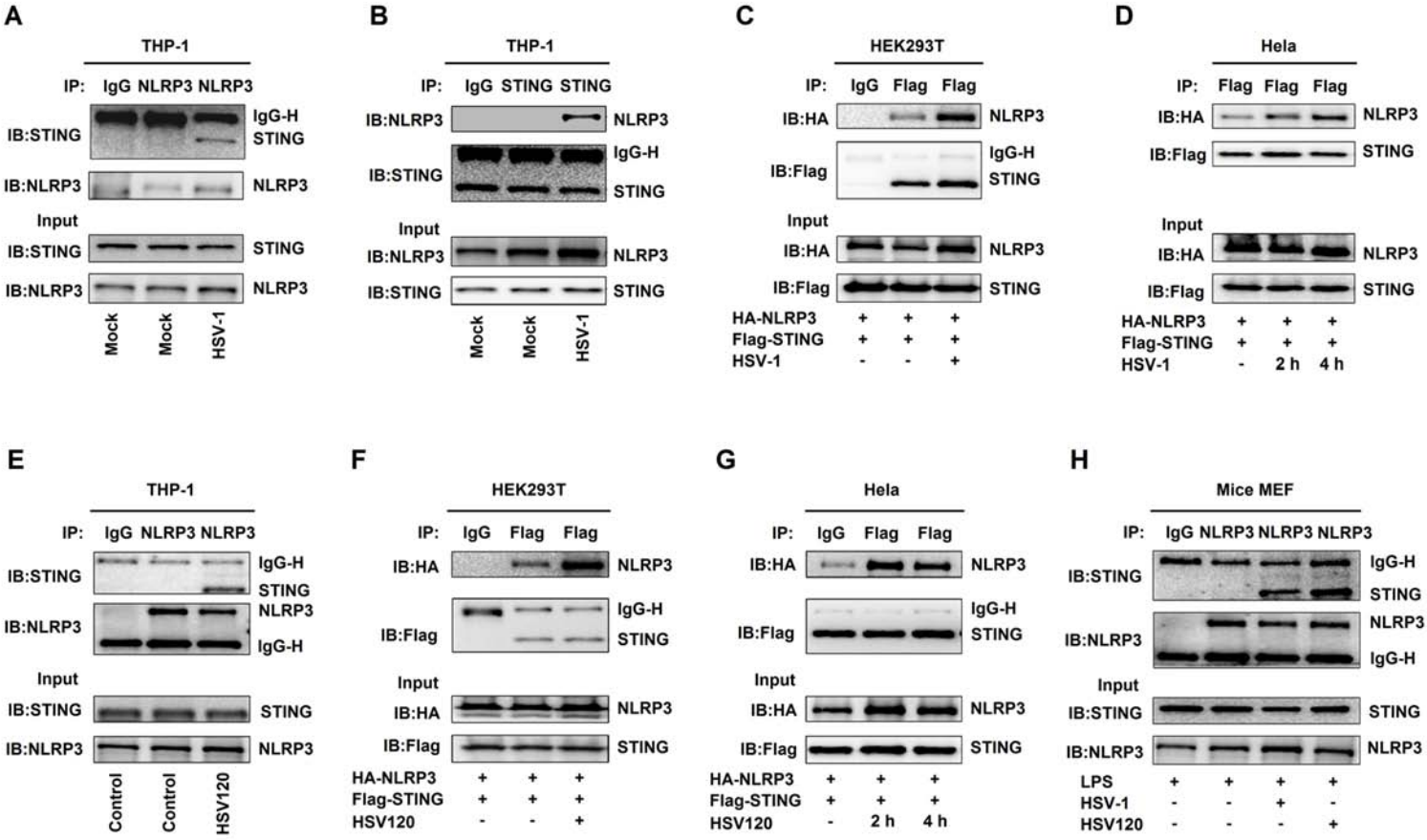
A
THP-1
IP: IgG NLRP3 NLRP3
IB:STING
IgG-H
STING
IB:NLRP3
NLRP3
Input
IB:STING
STING
IB:NLRP3
NLRP3
Mock Mock HSV-1
B
THP-1
IP: IgG STING STING
IB:NLRP3
NLRP3
IB:STING
IgG-H
STING
Input
IB:NLRP3
NLRP3
IB:STING
STING
Mock Mock HSV-1
C
HEK293T
IP: IgG Flag Flag
IB:HA
NLRP3
IB:Flag
IgG-H
STING
Input
IB:HA
NLRP3
IB:Flag
STING
HA-NLRP3 + + +
Flag-STING + + +
HSV-1 - - +
D
Hela
IP: Flag Flag Flag
IB:HA
NLRP3
IB:Flag
STING
Input
IB:HA
NLRP3
IB:Flag
STING
HA-NLRP3 + + +
Flag-STING + + +
HSV-1 - 2 h 4 h
E
THP-1
IP: IgG NLRP3 NLRP3
IB:STING
IgG-H
STING
IB:NLRP3
NLRP3
IgG-H
Input
IB:STING
STING
IB:NLRP3
NLRP3
Control Control HSV120
F
HEK293T
IP: IgG Flag Flag
IB:HA
NLRP3
IB:Flag
IgG-H
STING
Input
IB:HA
NLRP3
IB:Flag
STING
HA-NLRP3 + + +
Flag-STING + + +
HSV120 - - +
G
Hela
IP: IgG Flag Flag
IB:HA
NLRP3
IB:Flag
IgG-H
STING
Input
IB:HA
NLRP3
IB:Flag
STING
HA-NLRP3 + + +
Flag-STING + + +
HSV120 - 2 h 4 h
H
Mice MEF
IP: IgG NLRP3 NLRP3 NLRP3
IB:STING
IgG-H
STING
IB:NLRP3
NLRP3
IgG-H
Input
IB:STING
STING
IB:NLRP3
NLRP3
LPS + + + +
HSV-1 - - + -
HSV120 - - - +

Figure 3

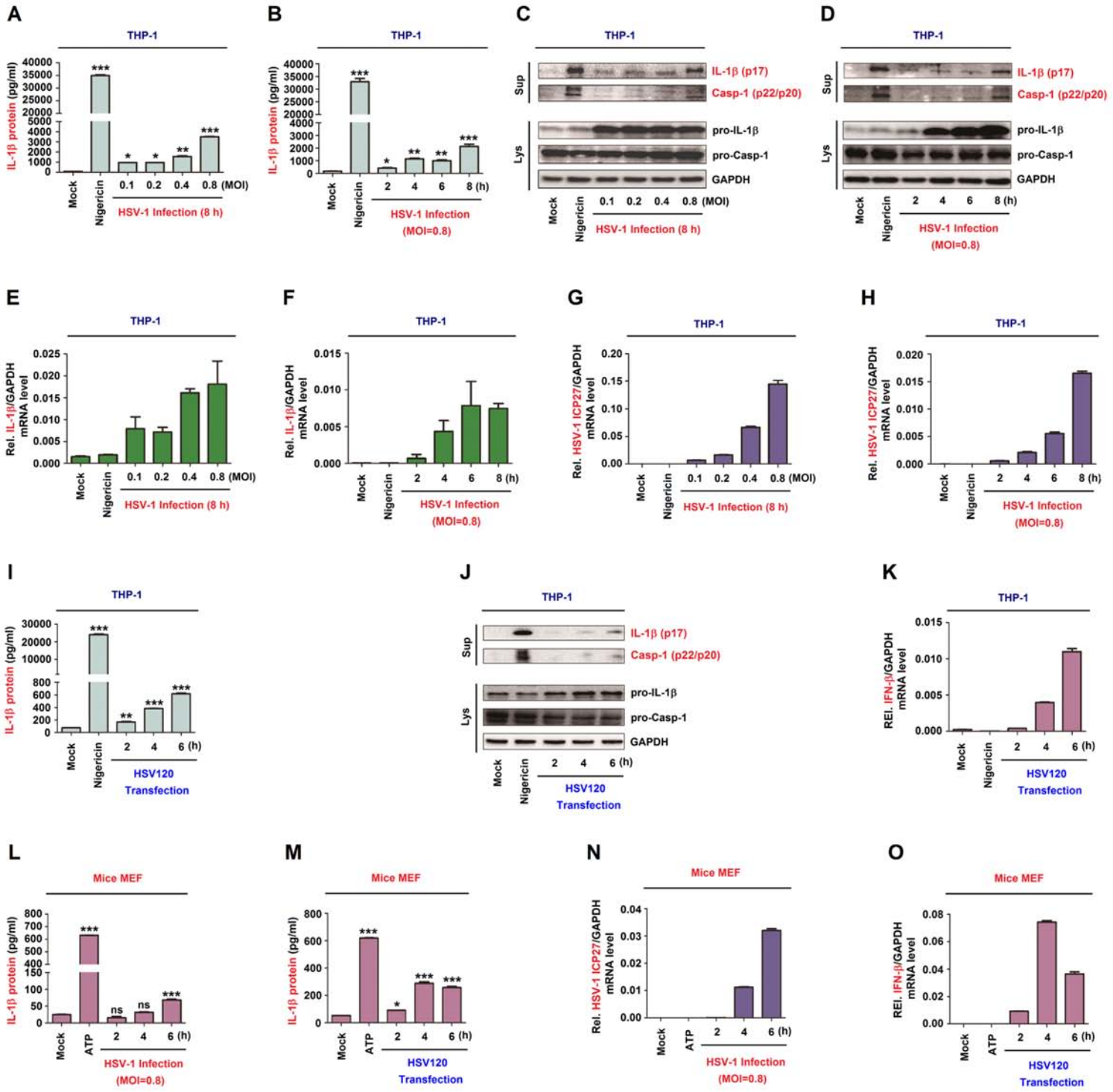
A
THP-1
IL-1β protein (pg/ml)
Mock
Nigericin
0.1 0.2 0.4 0.8 (MOI)
HSV-1 Infection (8 h)
B
THP-1
IL-1β protein (pg/ml)
Mock
Nigericin
2 4 6 8 (h)
HSV-1 Infection
(MOI=0.8)
C
THP-1
Sup
Lys
IL-1β (p17)
Casp-1 (p22/p20)
pro-IL-1β
pro-Casp-1
GAPDH
Mock
Nigericin
0.1 0.2 0.4 0.8 (MOI)
HSV-1 Infection (8 h)
D
THP-1
Sup
Lys
IL-1β (p17)
Casp-1 (p22/p20)
pro-IL-1β
pro-Casp-1
GAPDH
Mock
Nigericin
2 4 6 8 (h)
HSV-1 Infection
(MOI=0.8)
E
THP-1
Rel. IL-1β/GAPDH mRNA level
Mock
Nigericin
0.1 0.2 0.4 0.8 (MOI)
HSV-1 Infection (8 h)
F
THP-1
Rel. IL-1β/GAPDH mRNA level
Mock
Nigericin
2 4 6 8 (h)
HSV-1 Infection
(MOI=0.8)
G
THP-1
Rel. HSV-1 ICP27/GAPDH mRNA level
Mock
Nigericin
0.1 0.2 0.4 0.8 (MOI)
HSV-1 Infection (8 h)
H
THP-1
Rel. HSV-1 ICP27/GAPDH mRNA level
Mock
Nigericin
2 4 6 8 (h)
HSV-1 Infection
(MOI=0.8)
I
THP-1
IL-1β protein (pg/ml)
Mock
Nigericin
2 4 6 (h)
HSV120
Transfection
J
THP-1
Sup
Lys
IL-1β (p17)
Casp-1 (p22/p20)
pro-IL-1β
pro-Casp-1
GAPDH
Mock
Nigericin
2 4 6 (h)
HSV120
Transfection
K
THP-1
REl. IFN-β/GAPDH mRNA level
Mock
Nigericin
2 4 6 (h)
HSV120
Transfection
L
Mice MEF
IL-1β protein (pg/ml)
Mock
ATP
2 4 6 (h)
HSV-1 Infection
(MOI=0.8)
M
Mice MEF
IL-1β protein (pg/ml)
Mock
ATP
2 4 6 (h)
HSV120
Transfection
N
Mice MEF
Rel. HSV-1 ICP27/GAPDH mRNA level
Mock
ATP
2 4 6 (h)
HSV-1 Infection
(MOI=0.8)
O
Mice MEF
REl. IFN-β/GAPDH mRNA level
Mock
ATP
2 4 6 (h)
HSV120
Transfection

Figure 4

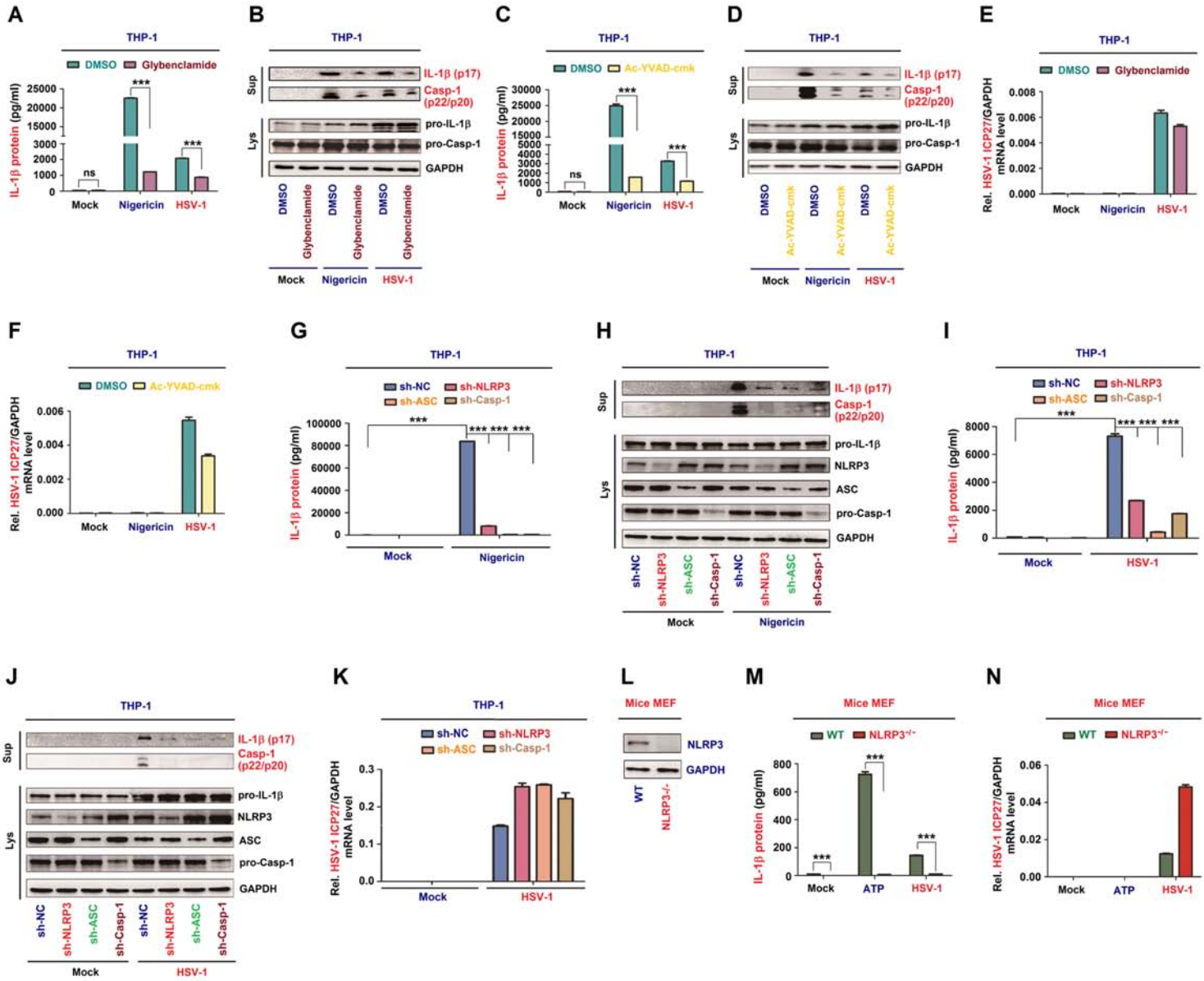
A
THP-1
DMSO
Glybenclamide
IL-1β protein (pg/ml)
ns
***
Mock
Nigericin
HSV-1
B
THP-1
Sup
Lys
IL-1β (p17)
Casp-1 (p22/p20)
pro-IL-1β
pro-Casp-1
GAPDH
DMSO
Glybenclamide
Mock
Nigericin
HSV-1
C
THP-1
DMSO
Ac-YVAD-cmk
IL-1β protein (pg/ml)
D
THP-1
Ac-YVAD-cmk
E
THP-1
Rel. HSV-1 ICP27/GAPDH mRNA level
F
THP-1
G
THP-1
sh-NC
sh-NLRP3
sh-ASC
sh-Casp-1
H
THP-1
NLRP3
ASC
I
THP-1
J
THP-1
K
THP-1
L
Mice MEF
WT
NLRP3-/-
M
Mice MEF
ATP
N
Mice MEF

Figure 5

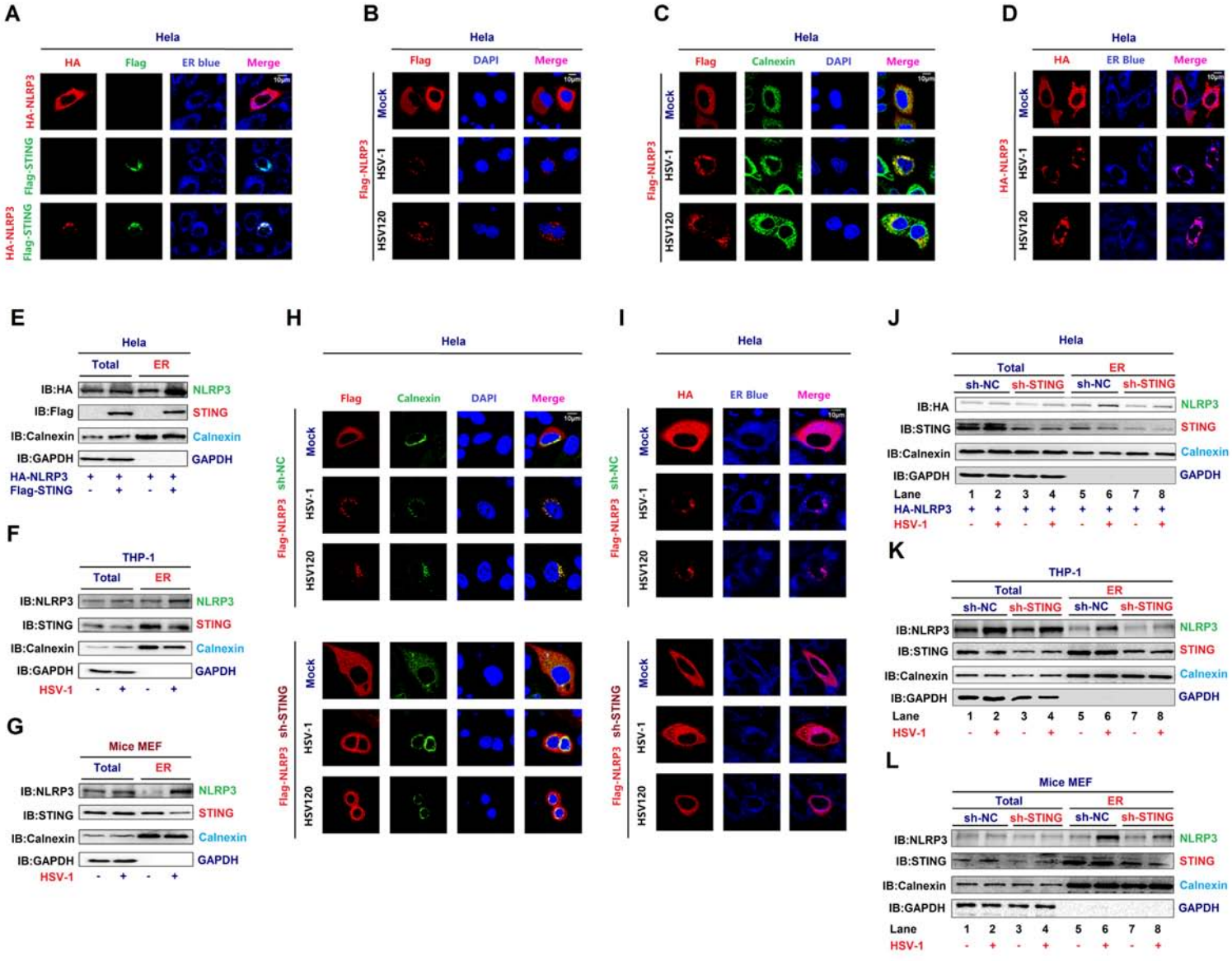
A
Hela
HA
Flag
ER blue
Merge
HA-NLRP3
Flag-STING
B
Hela
Flag
DAPI
Merge
Flag-NLRP3
Mock
HSV-1
HSV120
C
Hela
Flag
Calnexin
DAPI
Merge
D
Hela
HA
ER Blue
Merge
E
Hela
Total
ER
IB:HA
IB:Flag
IB:Calnexin
IB:GAPDH
NLRP3
STING
Calnexin
GAPDH
HA-NLRP3
Flag-STING
F
THP-1
IB:NLRP3
IB:STING
HSV-1
G
Mice MEF
H
I
J
sh-NC
sh-STING
Lane
K
L

Figure 6

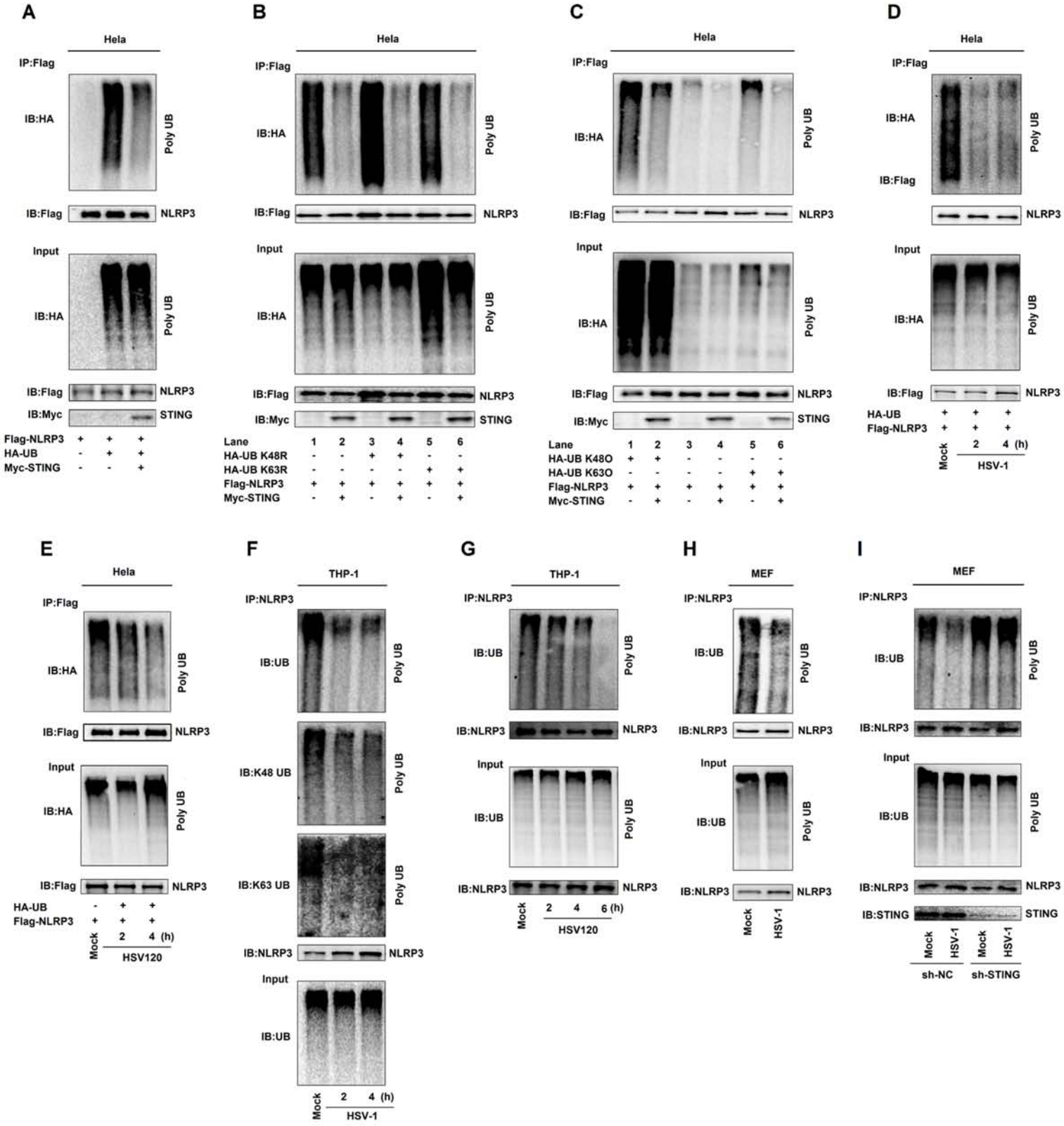
A
Hela
IP:Flag
IB:HA
Poly UB
IB:Flag
NLRP3
Input
IB:HA
Poly UB
IB:Flag
NLRP3
IB:Myc
STING
Flag-NLRP3 + + +
HA-UB - + +
Myc-STING - - +
B
Hela
IP:Flag
IB:HA
Poly UB
IB:Flag
NLRP3
Input
IB:HA
Poly UB
IB:Flag
NLRP3
IB:Myc
STING
Lane 1 2 3 4 5 6
HA-UB K48R - - + + - -
HA-UB K63R - - - - + +
Flag-NLRP3 + + + + + +
Myc-STING - + - + - +
C
Hela
IP:Flag
IB:HA
Poly UB
IB:Flag
NLRP3
Input
IB:HA
Poly UB
IB:Flag
NLRP3
IB:Myc
STING
Lane 1 2 3 4 5 6
HA-UB K48O + + - - - -
HA-UB K63O - - - - + +
Flag-NLRP3 + + + + + +
Myc-STING - + - + - +
D
Hela
IP:Flag
IB:HA
IB:Flag
Poly UB
NLRP3
Input
IB:HA
Poly UB
IB:Flag
NLRP3
HA-UB + + +
Flag-NLRP3 + + +
Mock 2 4 (h)
HSV-1
E
Hela
IP:Flag
IB:HA
Poly UB
IB:Flag
NLRP3
Input
IB:HA
Poly UB
IB:Flag
NLRP3
HA-UB - + +
Flag-NLRP3 + + +
Mock 2 4 (h)
HSV120
F
THP-1
IP:NLRP3
IB:UB
Poly UB
IB:K48 UB
Poly UB
IB:K63 UB
Poly UB
IB:NLRP3
NLRP3
Input
IB:UB
Mock 2 4 (h)
HSV-1
G
THP-1
IP:NLRP3
IB:UB
Poly UB
IB:NLRP3
NLRP3
Input
IB:UB
Poly UB
IB:NLRP3
NLRP3
Mock 2 4 6 (h)
HSV120
H
MEF
IP:NLRP3
IB:UB
Poly UB
IB:NLRP3
NLRP3
Input
IB:UB
Poly UB
IB:NLRP3
NLRP3
Mock
HSV-1
I
MEF
IP:NLRP3
IB:UB
Poly UB
IB:NLRP3
NLRP3
Input
IB:UB
Poly UB
IB:NLRP3
NLRP3
IB:STING
STING
Mock HSV-1 Mock HSV-1
sh-NC
sh-STING

Figure 7

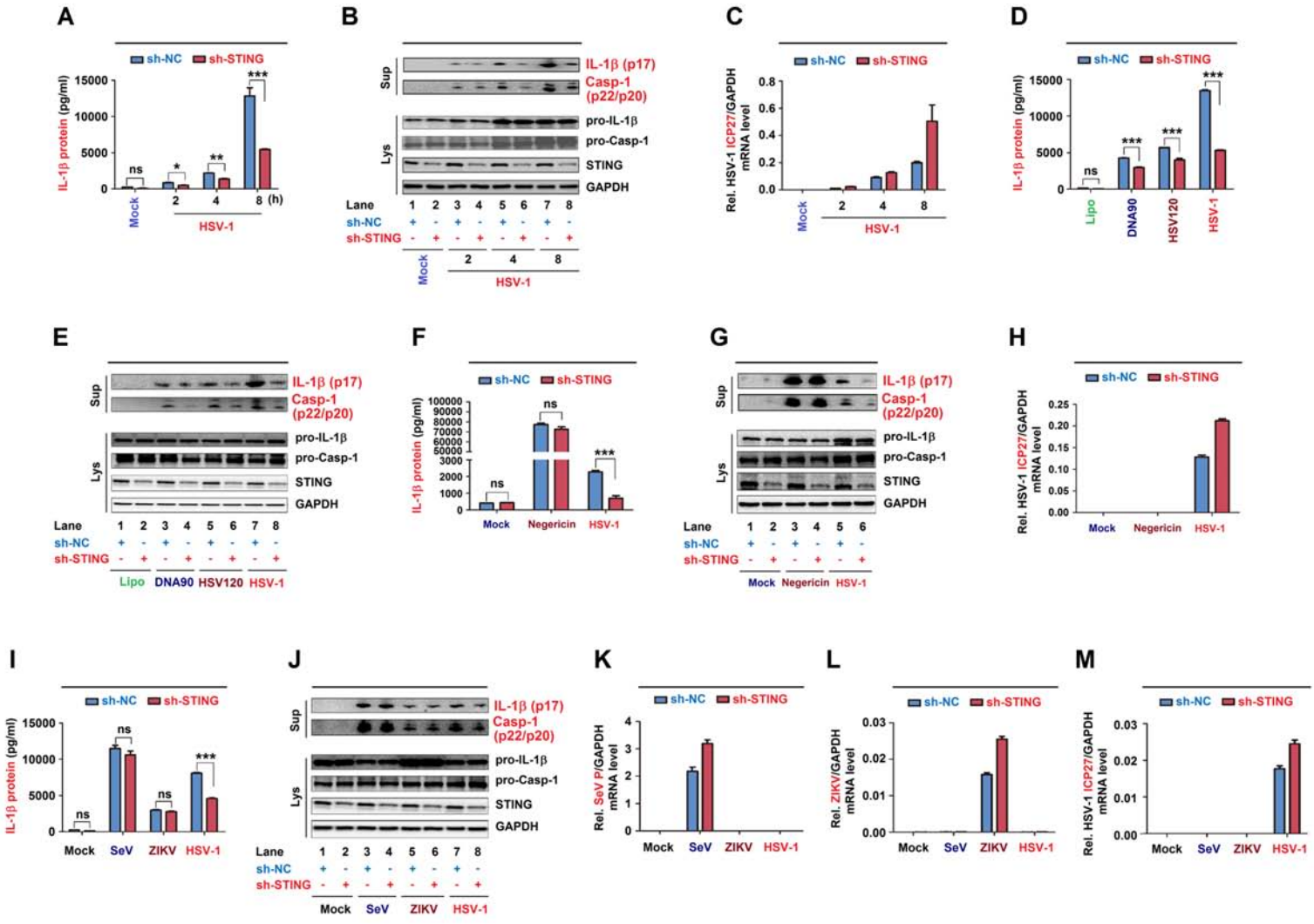
A
sh-NC
sh-STING
IL-1β protein (pg/ml)
15000
10000
5000
0
ns
*
**
***
Mock
2
4
8 (h)
HSV-1
B
Sup
Lys
IL-1β (p17)
Casp-1 (p22/p20)
pro-IL-1β
pro-Casp-1
STING
GAPDH
Lane 1 2 3 4 5 6 7 8
sh-NC + - + - + - + -
sh-STING - + - + - + - +
Mock
2
4
8
HSV-1
C
sh-NC
sh-STING
Rel. HSV-1 ICP27/GAPDH mRNA level
0.8
0.6
0.4
0.2
0.0
Mock
2
4
8
HSV-1
D
sh-NC
sh-STING
IL-1β protein (pg/ml)
15000
10000
5000
0
ns
***
***
***
Lipo
DNA90
HSV120
HSV-1
E
Sup
Lys
IL-1β (p17)
Casp-1 (p22/p20)
pro-IL-1β
pro-Casp-1
STING
GAPDH
Lane 1 2 3 4 5 6 7 8
sh-NC + - + - + - + -
sh-STING - + - + - + - +
Lipo
DNA90
HSV120
HSV-1
F
sh-NC
sh-STING
IL-1β protein (pg/ml)
100000
90000
80000
70000
60000
50000
3000
2000
1000
0
ns
ns
***
Mock
Negericin
HSV-1
G
Sup
Lys
IL-1β (p17)
Casp-1 (p22/p20)
pro-IL-1β
pro-Casp-1
STING
GAPDH
Lane 1 2 3 4 5 6
sh-NC + - + - + -
sh-STING - + - + - +
Mock
Negericin
HSV-1
H
sh-NC
sh-STING
Rel. HSV-1 ICP27/GAPDH mRNA level
0.25
0.20
0.15
0.10
0.05
0.00
Mock
Negericin
HSV-1
I
sh-NC
sh-STING
IL-1β protein (pg/ml)
15000
10000
5000
0
ns
ns
ns
***
Mock
SeV
ZIKV
HSV-1
J
Sup
Lys
IL-1β (p17)
Casp-1 (p22/p20)
pro-IL-1β
pro-Casp-1
STING
GAPDH
Lane 1 2 3 4 5 6 7 8
sh-NC + - + - + - + -
sh-STING - + - + - + - +
Mock
SeV
ZIKV
HSV-1
K
sh-NC
sh-STING
Rel. SeV P/GAPDH mRNA level
4
3
2
1
0
Mock
SeV
ZIKV
HSV-1
L
sh-NC
sh-STING
Rel. ZIKV/GAPDH mRNA level
0.03
0.02
0.01
0.00
Mock
SeV
ZIKV
HSV-1
M
sh-NC
sh-STING
Rel. HSV-1 ICP27/GAPDH mRNA level
0.03
0.02
0.01
0.00
Mock
SeV
ZIKV
HSV-1

Figure 8

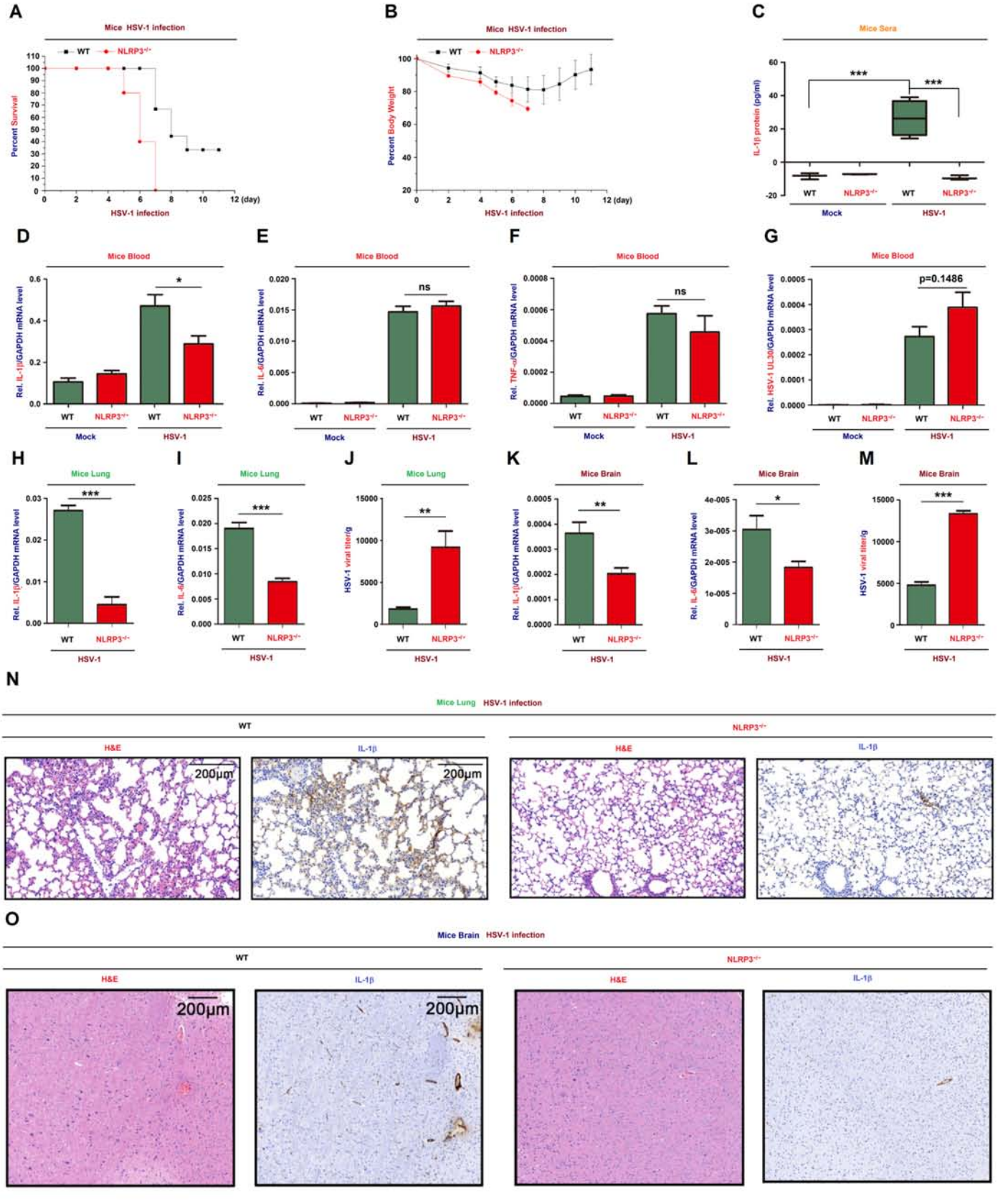
A
Mice HSV-1 infection
WT
NLRP3-/-
Percent Survival
HSV-1 infection
12 (day)
B
Mice HSV-1 infection
Percent Body Weight
C
Mice Sera
IL-1β protein (pg/ml)
***
Mock
HSV-1
D
Mice Blood
Rel. IL-1β/GAPDH mRNA level
*
E
Mice Blood
Rel. IL-6/GAPDH mRNA level
ns
F
Mice Blood
Rel. TNF-α/GAPDH mRNA level
ns
G
Mice Blood
Rel. HSV-1 UL30/GAPDH mRNA level
p=0.1486
H
Mice Lung
Rel. IL-1β/GAPDH mRNA level
***
I
Mice Lung
Rel. IL-6/GAPDH mRNA level
***
J
Mice Lung
HSV-1 viral titer/g
**
K
Mice Brain
Rel. IL-1β/GAPDH mRNA level
**
L
Mice Brain
Rel. IL-6/GAPDH mRNA level
*
M
Mice Brain
HSV-1 viral titer/g
***
N
Mice Lung HSV-1 infection
WT
NLRP3-/-
H&E
IL-1β
200μm
O
Mice Brain HSV-1 infection
WT
NLRP3-/-
H&E
IL-1β
200μm

Figure 9

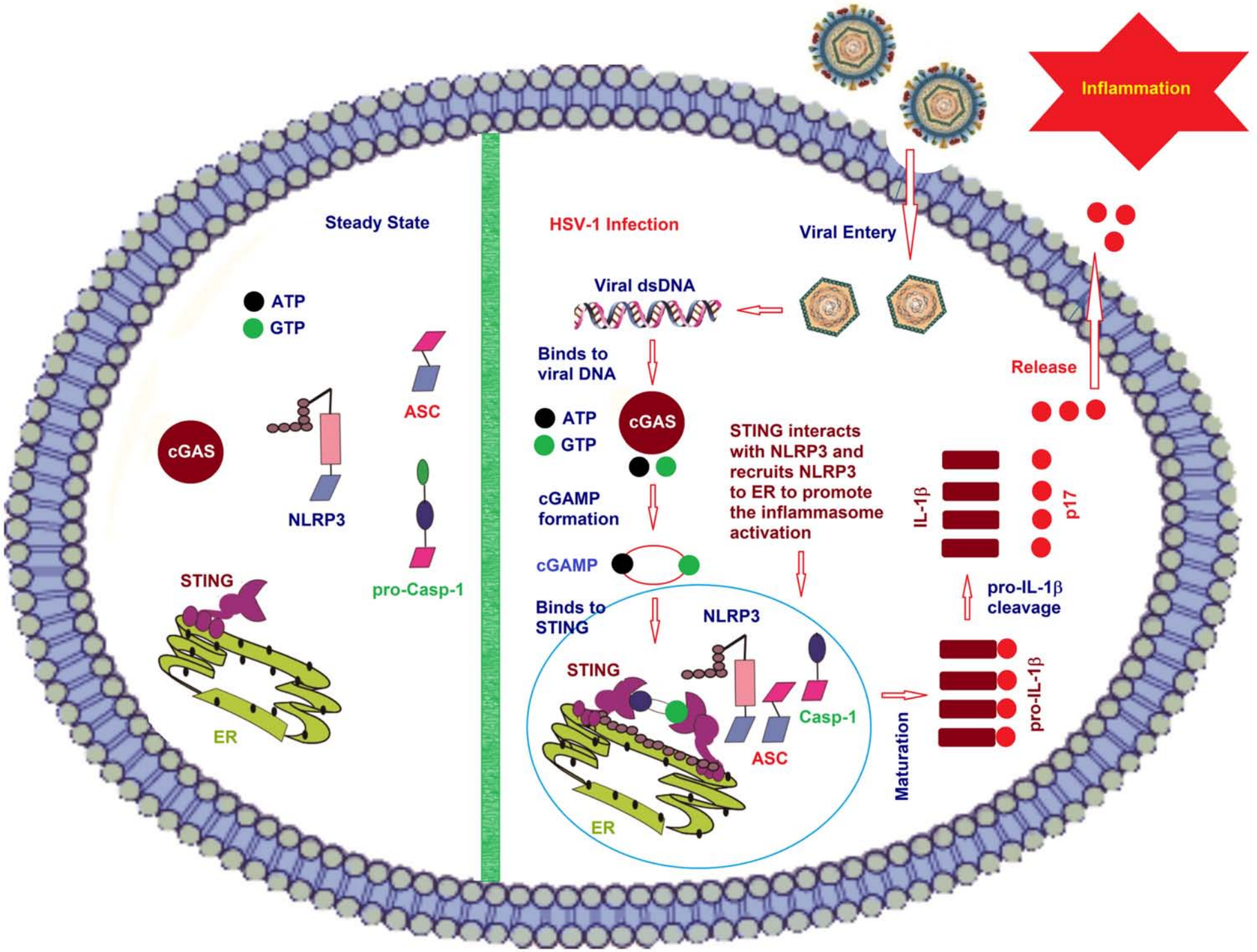
Inflammation
Steady State
HSV-1 Infection
Viral Entery
Viral dsDNA
ATP
GTP
Binds to viral DNA
cGAS
ASC
NLRP3
pro-Casp-1
STING
ER
cGAMP formation
cGAMP
STING interacts with NLRP3 and recruits NLRP3 to ER to promote the inflammasome activation
Binds to STING
Casp-1
Release
IL-1β
p17
pro-IL-1β cleavage
pro-IL-1β
Maturation